Universidad
Carlos III de Madrid
www.uc3m.es

Tesis Doctoral

EXPERIMENTAL STUDY AND MONTE CARLO MODELING OF OBJECT MOTION IN A BUBBLING FLUIDIZED BED

Autor
Luis Miguel García Gutiérrez

Director
Ulpiano Ruiz-Rivas Hernando
Co-director
Antonio Soria Verdugo

DEPARTAMENTO DE INGENIERÍA TÉRMICA Y DE FLUIDOS

Leganés (Madrid), julio 2014

Tesis doctoral

EXPERIMENTAL STUDY AND MONTE CARLO MODELING OF OBJECT MOTION IN A BUBBLING FLUIDIZED BED

Autor: Luis Miguel García Gutiérrez

Director de Tesis: Ulpiano Ruiz-Rivas Hernando
Co-director de Tesis: Antonio Soria Verdugo

Firma del Tribunal Calificador:

Firma

Presidente: D. Bo Leckner, Chalmers University of Technology

Secretario: D. José A. Almendros Ibáñez, Universidad de Castilla - La Mancha

Vocal: D. Jacobo Porteiro Fresco, Universidad de Vigo

Calificación:

Leganés (Madrid), 4 de julio de 2014

En memoria de mi abuelo y de mi tía

DEPARTAMENTO DE INGENIERÍA TÉRMICA Y DE FLUIDOS
Escuela Politécnica Superior

EXPERIMENTAL STUDY AND MONTE CARLO MODELING OF OBJECT MOTION IN A BUBBLING FLUIDIZED BED

Autor
Luis Miguel García Gutiérrez

Director de Tesis
Ulpiano Ruiz-Rivas Hernando
Co-director de Tesis
Antonio Soria Verdugo

Leganés (Madrid), julio 2014

Un ínfimo paso para la humanidad,
pero un gran paso para mí
Anónimo

. . .
Nunca te entregues ni te apartes
junto al camino, nunca digas
no puedo más y aquí me quedo.
. . .
Palabras para Julia (José Agustín Goytisolo)

Agradecimientos

Después de haber redactado toda la tesis, ha llegado el momento de escribir los agradecimientos. En primer lugar, me gustaría agradecérsela a mis abuelas, han sabido sobreponerse ante las adversidades y son un claro ejemplo de lucha por vivir. A mis padres, no tuvieron la oportunidad de poder estudiar y sin embargo consiguieron, a base de trabajo y más trabajo, que sus hijos sí la tuvieran. A mi hermana, por mostrarme que no existe ninguna barrera que ella no sea capaz de superar. Al resto de mi familia, tí@s, prim@s, no han olvidado cúales son sus raíces y eso hace que nos mantengamos unidos.

Aunque sea un tópico, en este caso está más que demostrado, que sin mis directores, Ulpiano y Antonio, esta tesis nunca la podría haber empezado y mucho menos haberla terminado. Gracias por el esfuerzo durante todo este tiempo para conseguir que se volviera una realidad, y por enseñarme y compartir tanto durante esta etapa de mi vida.

Quería agradecer también a los doctores permanentes del grupo ISE, Antonio Acosta, Domingo, Javi, María, Mercedes y especialmente a Néstor, por darme la oportunidad de realizar la tesis y por el apoyo y colaboración durante todo este tiempo. Al resto de doctores del grupo, Carol, Celia, Sergio, por los tantos momentos compartidos dentro y fuera de la universidad. No me puedo olvidar de Fernando, porque empezamos juntos la carrera hace años y aquí seguimos, a pesar del tiempo, amigos como el primer día. A los demás miembros del grupo, Luis y María, mis compañeros de despacho y de gran parte del tiempo de mi vida durante este periodo, por compartir tantos ratos únicos dentro del despacho. A Alberto, Dani S y Edu, compañeros de Iterate F.C., a Lucía, por todo el tiempo que le he robado por haber compartido directores, a Javi S y Jesús, por ayudarme en el laboratorio siempre que lo he necesitado a pesar de los pesares, a Reyes, que le devolviste la sonrisa y haces que la siga teniendo. Agradecer a todos los miembros del grupo de Mecánica de Fluidos su ayuda con los equipos de medida e iluminación, y en especial a sus doctorandos, Alberto, Dani, Paula, a Ana, que empezó conmigo el doctorado y hemos ido siempre a la par, ánimo que ya no queda nada, a Wil, aunque ya no es doctorando, por compartir lo que es suyo sin pedir nada a cambio, a Elena, no puedo olvidarme de ella o no entro en casa, a Juan como miembro consejero, en todos los temas, del despacho 1.1.D23 y en particular a Mariano, que sin duda esta

tesis no se podría leer si no fuera por él y por su tiempo invertido; gracias por ayudarme a conseguirlo. A Cristina por su ayuda en todas las gestiones durante este tiempo relacionas y no relacionadas con la tesis. No me puedo olvidar de las personas que estaban cuando empecé y que por unas razones u otras ya no están, en especial a Jorge, por su grandeza en todos los sentidos. Gracias a los técnicos de laboratorio del departamento, por su disposición en todo momento en lo referente a la instalación experimental.

Me agustaría agradecer también a las personas de Chalmers, en Göteborg, lugar de mi estancia durante tres meses, su apoyo durante ese tiempo, en especial a Filip, a la comunidad española y ecuatoriana allí instalada que hicieron que mi estancia fuera más agradable, a Erik, mi compañero de ensayos y por supuesto a David Pallarès, mi tutor de la estancia, y algo más que un tutor, con el que compartí tantos momentos dentro y fuera de Chalmers, y los sigo compartiendo de vez en cuando desde la distancia.

Y como no, mi vida no tendría sentido, y por lo tanto mi tesis tampoco, sin ellos, mis amigos, aquellos con los que he compartido inolvidables experiencias desde hace más de 15 años, y lo más importante, que las sigo compartiendo. Esta tesis se ha conseguido gracias a vosotros, y por lo tanto, es parte vuestra.

Finalmente, estás tú, que me aguantas diariamente y haces que mi vida se me vuelva de colores, gracias por estar ahí y compartir tu vida conmigo.

Abstract

Fluidized beds are employed for a wide variety of applications such as drying, coating of particles, catalytic reactions, or thermal conversion processes. In a number of these applications, objects differing in density and/or size from the dense phase material are found in the bed. These objects can be agglomerates, catalysts or reactants. In this PhD thesis, a fundamental study of the motion of objects is presented, but considering also the main characteristics of the thermal conversion processes for these objects.

Fluidized beds are used for the thermal conversion of fuels with low heating value and/or large humidity content, applications in which the high heat and mass transfer exchange provided by fluidized beds becomes relevant. In general, fuel particles of such characteristics are much larger in size than the dense phase material, and have a density that can range between the density of the dense bed to rather smaller values. In all cases, a good mixing of the fuel particles throughout the bed involves a higher efficiency in the thermal conversion process.

In fluidized beds, the mixing rate in the vertical direction is higher than that in the lateral direction, as a result of the bubble motion. A proper distribution of the fuel particles in the whole bed is fundamental for an adequate development of the chemical reaction, and to avoid the formation of cold or hot spots. Therefore, the lateral mixing becomes a relevant parameter.

The lateral and vertical displacement of the fuel particle and the dimensions of the reactor have to be taken into account together with the fuel particle residence time in the bed for a proper characterization. The residence time of a fuel particle during its thermal conversion can be represented either by the devolatilization time or the char conversion time. For the purposes of this thesis, the first one will be used, as it is the limiting factor in time. Also, a comparison between the time that the fuel particle remains in the freeboard, the time it remains immersed in the bed, and the devolatilization time is relevant. Finally, a significant design parameter of reactors, the location and number of feeding ports for a proper distribution of the fuel throughout the bed, depends on the capacity of the fuel particle to move laterally.

In this dissertation, the main parameters that characterize the object motion in a bubbling fluidized bed are obtained experimentally and related to bed

variables such as the dimensionless gas velocity. These main parameters include the time that an object spends during its motion throughout the bed, either immersed in the dense bed or in the freeboard, and the vertical and lateral displacements. The experimental characterization, analyzing the dynamics of an object in a fluidized bed, provides the information to develop a model for the object motion. The model is divided in several sub-models, taking into account the different dynamics to which the object is subjected throughout the bed. In each case, the relevant parameters of the object motion, displacement and time, are found to relate to more elemental factors with definite statistical distributions, which are obtained experimentally. The different sub-models are based on the simulations of the relations between the statistical distributions of such factors using a Monte Carlo method.

The object behavior in a bubbling fluidized bed can be divided in two parts: when it is in the freeboard and when it is immersed in the dense bed. In the freeboard, a large object is only affected by the gravitational force; the drag force and the interactions with dense phase particles being negligible. Therefore, its motion can be characterized as a ballistic motion. This motion can be described by the object velocity at the instant of its ejection by the bubbles to the freeboard. Such a velocity can be characterized with statistical information of the modulus and angle, and modeled as a function of the bed operational conditions. On the other hand, the behavior of the object when it is immersed in the bed can still be divided in two different processes: a sinking process and a rising process. The sinking process is governed by the dense phase and thus the object moves according to its motion. This process can be defined by statistical parameters such as the probability of the object to attain a maximum depth or the probability of the object to start a rising process at each position during its sinking motion. In the rising process, the object is mainly affected by the bubbles, and the capacity of reaching the bed surface directly depends on its attachment to the bubbles. This behavior can be characterized by a parameter that represents the probability of an object to reach the surface directly when it starts a rising path and its opposite, the probability of detaching from the bubble and restart a sinking path before reaching the bed surface. As a result, the motion of the object either when it is in the freeboard or immersed in the dense bed can be described by the statistical parameters obtained experimentally, and models based on Monte Carlo simulations of such parameters can be derived.

Finally, the combination of the different sub-models of the object motion

throughout the bed permits to describe the global behavior of an object in a large-scale bubbling fluidized bed. A global model based on Monte Carlo simulations of the elemental parameters obtained experimentally is developed, based on the elemental statistical parameters of the object motion. The relevant parameters that describe the behavior of a fuel particle, the lateral and vertical displacement or the time spent during its motion throughout the bed, are determined using the model, and validated with experiments reported in the literature.

Resumen

Los lechos fludizados se emplean en una gran variedad de aplicaciones, tales como secado, recubrimiento de partículas, reacciones catalíticas o procesos de conversión térmica. En gran parte de estas aplicaciones, se pueden encontrar en el lecho objetos con tamaño diferente al del material de la fase densa. Estos objetos pueden ser aglomerados, catalizadores o reactivos. En esta tesis doctoral se presenta un estudio fundamental del movimiento de dichos objetos, teniendo en especial consideración las principales características de los procesos de conversión térmica en los que estos objetos pueden intervenir.

Los lechos fluidizados se usan habitualmente para la conversión térmica de combustibles con bajo poder calorífico y/o con alto contenido en humedad, aplicación en la cual el elevado intercambio de calor y de masa proporcionado por los lechos fluidizados resulta relevante. En general, las partículas de combustible son mucho mayores en tamaño que el material del lecho y tienen una densidad que varía entre la densidad del propio lecho y valores bastante menores. En todos los casos, un buen mezclado de las partículas de combustible en el lecho implica una mayor eficiencia en los procesos de conversión térmica.

En los lechos fluidizados el mezclado en la dirección vertical es mayor que en la dirección lateral a consecuencia del movimiento de las burbujas. Una distribución correcta de las partículas de combustible por todo el lecho es fundamental para un desarrollo adecuado de la reacción química y para evitar la formación de zonas frías y calientes. Por tanto, el mezclado lateral se convierte en un parámetro de gran importancia.

Tanto el desplazamiento lateral y vertical del combustible como las dimensiones del reactor han de ser tenidos en cuenta, junto con el tiempo de residencia en el lecho de las partículas de combustible, para una correcta caracterización de su funcionamiento. El tiempo de conversión de una partícula de combustible puede ser representado tanto por el tiempo de devolatilización como por el tiempo de conversión del char. En línea con el objetivo de la tesis, se usará el primero, ya que es el factor limitante en tiempo. Finalmente, la localización y el número de alimentadores de combustible necesarios para una correcta distribución del combustible en todo el lecho, parámetro significativo en el diseño de reactores, depende fundamentalmente de la capacidad de las partículas de combustible para moverse lateralmente.

En esta tesis se obtienen experimentalmente los principales parámetros que caracterizan el movimiento de un objeto en un lecho fluidizado burbujeante, relacionándolos con variables características del lecho, como la relación entre la velocidad del gas y la velocidad de mínima fluidización. Estos parámetros principales, son por un lado, el tiempo que el objeto invierte durante su movimiento a través del lecho y, por otro lado, su desplazamiento vertical y lateral, ambos identificados de forma separada tanto en el interior del lecho como en la superficie libre. La caracterización experimental de la dinámica de un objeto en un lecho fluidizado y de los factores relevantes permite desarrollar un modelo del movimiento del objeto. El modelo se dividirá en varios submodelos que expliquen las diferentes dinámicas que sigue el objeto a través del lecho. En cada caso, se obtendrán los parámetros relevantes del movimiento del objeto, desplazamiento y tiempo, relacionándolos con factores más elementales cuyas distribuciones estadísticas puedan ser obtenidas experimentalmente. Los diferentes submodelos se basan en simulaciones de las relaciones entre las distribuciones estadísticas de dichos factores, usando para ello el método de Monte Carlo.

Para su estudio y modelado, el movimiento de un objeto en un lecho fluidizado burbujeante puede dividirse en dos partes: cuando está en la superficie libre y cuando está inmerso en el lecho. En la superficie libre, en comparación con la fase densa, un objeto grande se ve afectado únicamente por la fuerza gravitacional, ya que la fuerza de arrastre del gas y la interacción con partículas de fase densa resultan despreciables. Por lo tanto, su movimiento será un movimiento balístico. Este movimiento queda descrito por la velocidad del objeto en el instante de su eyección a la superficie libre por parte de las burbujas. Dicha velocidad puede ser caracterizada con información estadística de su módulo y ángulo, y modelada en función de los parámetros del lecho. Por otro lado, el comportamiento del objeto cuando se encuentra inmerso en el lecho puede separarse también en dos procesos de características muy diferentes: un proceso de subida y un proceso de bajada. El proceso de bajada está gobernado por la interacción con la fase densa, moviéndose por tanto el objeto solidariamente a ésta. Su comportamiento durante ese proceso puede definirse mediante parámetros estadísticos como la probabilidad del objeto de alcanzar diferentes profundidades máximas o la probabilidad de que el objeto comience un proceso de subida a partir de una determinada posición durante su movimiento de bajada. En el proceso de subida, el objeto se ve afectado principalmente por las burbujas y su capacidad de elevarse directamente hasta

la superficie del lecho depende del acoplamiento con éstas. Su comportamiento durante ese proceso puede ser caracterizado por un parámetro que represente la probabilidad de un objeto de alcanzar directamente la superficie del lecho cuando empieza un proceso de subida o, a la inversa, la probabilidad que tiene el objeto de desacoplarse de la burbuja y empezar un nuevo proceso de bajada antes de alcanzar la superficie del lecho. Como resultado, el movimiento del objeto tanto cuando está en la superficie libre como cuando se encuentra inmerso en el lecho se puede describir mediante parámetros estadísticos obtenidos experimentalmente, y modelar mediante el uso de simulaciones de Monte Carlo.

Finalmente, la combinación de los diferentes submodelos del movimiento del objeto a través del lecho permite describir el comportamiento global de un objeto en un lecho fluidizado burbujeante de escala industrial. Se ha desarrollado un modelo global basado en simulaciones de Monte Carlo de los parámetros elementales, empleando para ello los parámetros estadísticos representativos del movimiento del objeto, obtenidos experimentalmente. El modelo desarrollado permite obtener los parámetros relevantes que describen el comportamiento de una partícula de combustible; los desplazamientos lateral y vertical y el tiempo invertido en su movimiento a través del lecho. Los parámetros obtenidos son validados usando resultados experimentales disponibles en la literatura.

Contents

List of Figures

List of Tables

CHAPTER

ONE

Introduction: the motion of objects in fluidized beds

Contents

The efficiency of the thermal conversion of solid fuels depends strongly on the characteristics of the technology employed. Fluidized beds are used in many applications in industrial processes because of their high heat and mass transfer capacity. The high volumetric transfer area, homogeneous temperature, and high mixing rate, make fluidized bed reactors optimal for the chemical transformation of solid fuels, an specially for low-quality fuels.

For such an application, the design and characterization of fluidized bed reactors involves two major steps: the study of the fluidized bed dynamics and heat transfer, and the study of the kinetics of the fuel conversion processes. In the former, the dynamics of objects immersed in the bed, but different in size, shape and/or density to the dense phase material (the fuel particles) become of paramount importance.

In this PhD thesis, the behavior of large objects in a fluidized bed was analyzed. This thesis follows the research line initiated in previous works (Soria-Verdugo *et al.*, 2011*a*,*b*), being the author of this PhD thesis, coauthor of these works. This PhD thesis is a fundamental study on the motion of large objects in fluidized beds. Nevertheless, the results allow to characterize the main parameters of the performance of fludized bed reactors.

1.1 Background

Several authors have studied the behavior of objects in bubbling fluidized beds, employing different experimental techniques in 2-D and 3-D facilities. These studies can be divided in two main groups: objects with size and density similar to the dense phase material, and thus tracers of the dense phase, and objects larger than the dense phase material. We will focus on the latter category. These objects will have a circulation inside the dense bed determined by a complex dynamics, which includes sinking forces related with the dense phase motion, rising forces related with the bubbles, buoyancy forces due to differences in density and/or size with the dense bed and a motion in the freeboard affected by gravity and the gas drag force.

The first studies concerning the motion of large objects in fluidized beds were reviewed by Kunii & Levenspiel (1991) showing different behaviors as a function of the density of the objects. They reported that a large cylinder immersed in the bed was lifted to the surface of the bed in the roof of the bubble, although sometimes the object can also be raised in its wake. This behavior was observed for objects with a wide range of densities (800-1700 kg/m^3) in a bed with a bulk density around 1500 kg/m^3. On the other hand, objects with a density lower than 800 kg/m^3 rose to the surface of the bed in the roof of the bubbles and remained there, whereas objects with a density higher than 1700 kg/m^3 sank to the bottom of the bed and stayed there. Concerning the sinking process, they reported that the object velocity was similar to the downwards velocity of the dense phase. The influence of the buoyancy force was also analyzed by Nguyen & Grace (1978) for objects with different sizes, shapes and densities. They also determined the force suffered by the objects immersed in the bed due to the passing bubbles. They concluded that the force on an object in the upwards and downwards motion had similar magnitude but was applied during a longer period in the downwards process.

Rios *et al.* (1986) studied the vertical motion of large objects in 2-D and 3-D beds and discussed the sinking and rising processes using radioactive tracers. In their experiments, the density, size and shape of the large objects were varied for a range of gas velocities, bed heights and dense phase particle diameters. Their results confirmed that a large particle with a density similar to the dense bed moves throughout the whole bed, while for lower and higher densities, the object floats at the surface of the bed or remains over the distributor respectively. Furthermore, they observed that, in the rising process, a large object

was lifted to the surface of the bed following a series of small paths, defined as jerks, which were due to successive passing bubbles. Lim & Agarwal (1994) characterized the patterns of a large particle throughout the bed for a range of gas velocities, employing a tracking technique based on digital image analysis. They observed that the object sank at the sides of the bed while the rising process occurred in the preferential path of the bubbles, at the middle of the bed. The upwards velocity of the object in the rising process was determined experimentally by these authors, obtaining a value of 30% the mean bubble velocity. The downwards velocity of the object was also calculated and the results showed similar values to the downwards velocity of the dense phase. The rising velocity of large objects was also associated with the bubbles velocity by Rees *et al.* (2005). They studied the rise of a buoyant sphere in a 3-D fluidized bed varying its size and density. In the experiments, they observed that the rising velocity of the sphere was lower than the bubbles velocity, around 10%. The works of Pallarès & Johnsson (2006) and Pallarès *et al.* (2007) analyzed the motion of a phosphorescent particle in a 2-D bed for several bed aspect ratio configurations. They observed that a dense phase particle rises in the bubble wake directly to the bed surface, whereas when the object is far larger than the bed material, a detachment of the object from the bubble is often observed. They also studied the lateral motion of large particles in a 2-D bed and in a large scale 3-D fluidized bed (Olsson *et al.*, 2012). These works associated the lateral motion of objects with the structures developed by the different bubble paths. In the experimental works reported by Soria-Verdugo *et al.* (2011*a*,*b*,*c*) the motion of objects in 2-D and lab-scale 3-D fluidized beds was described, employing a tracking technique based on digital image analysis. They confirmed that an object sinks at the sides of the bed with a velocity similar to the dense phase, and rises in the middle of the bed with a rising velocity that in their case was observed to be around 20% the mean bubble velocity. Furthermore, they characterized the jerky behavior of an object in the rising process, reported by Rios *et al.* (1986), with statistical parameters that describe the probability of the objects to reach the surface directly. This characterization is valid for a wide variety of objects characteristics, bed heights, gas velocities and diameters of the dense phase particles. The time spent by an object during its motion when it is immersed in the bed was also calculated in a 2-D bed and in a lab-scale 3-D bed, varying the size and density of the object.

There is a general agreement in some aspects of the object motion. Nienow *et al.* (1978), Rios *et al.* (1986), Lim & Agarwal (1994), Rees *et al.* (2005) and

Soria-Verdugo *et al.* (2011*b*) studied the sinking and rising processes and their characteristic velocities, showing a good agreement between the sinking velocity and the dense phase velocity, while the rising velocity varied between authors from 10% to 30% the mean bubble velocity.

The buoyancy effects may or may not be significant depending on the bed and object characteristics and on the operational conditions of the bed. In general, fuel particles have lower densities than the dense bed, showing a flotsam behavior in fluidized beds. Even for denser fuels that circulate throughout the whole bed, when the devolatilization process occurs, the volatile matter escapes from the particle varying its properties and the particles tend to lift to the surface of the bed and remain there (Fiorentino *et al.*, 1997; Bruni *et al.*, 2002; Gómez-Barea & Leckner, 2010). A gas velocity increase can minimize this flotsam behavior, resulting in a proper circulation of the fuel particle throughout the bed (Wirsum *et al.*, 2001; Zhang *et al.*, 2009; Bai *et al.*, 2013). Soria-Verdugo *et al.* (2011*a*) characterized the limits of a proper circulation for an object as a function of its size and density, and the fluidization gas velocity.

Fluidized beds are characterized by a higher mixing rate in the vertical direction than in the lateral direction (Ito *et al.*, 1999; Gómez-Barea & Leckner, 2010), but the latter may be relevant in some applications. Pallarès & Johnsson (2006) observed the influence of bubble paths in the lateral motion of objects using a tracking technique in a 2-D bubbling fluidized bed. They showed that two solid mixing vortices are produced around each preferential bubble path at the middle of the vortices. In the case of 3-D beds, a toroidal flow can be found around the bubble preferential path. These bubble paths are affected by the operational conditions, the pressure drop of the distributor and the characteristics of the bed material. In a narrow 2-D bed, just one bubble path is observed at the center of the bed, while for wider beds other bubble paths appear and the configuration with two mixing vortices around the bubble path is repeated, in what is called a mixing cell (Pallarès *et al.*, 2007). The interchange of particles between different mixing cells generates a net particle lateral motion.

1.2 Previous works related to this thesis

The object behavior inside the dense bed was studied experimentally in previous works by Soria-Verdugo *et al.* (2011*a*,*b*). Their work is closely linked to the one carried out in this thesis. Some parameters obtained from those experiments were used in this PhD thesis as input data. Therefore, a detailed explanation of

these parameters will be carried out in this section. As stated in the previous section (1.1), Soria-Verdugo *et al.* (2011*b*) characterized the motion of an object in a 2-D bubbling fluidized bed with a tracking technique using digital image analysis for several dimensionless gas velocities, U/U_{mf}. The object employed in the experiments was a biomass pellet with a density of 1508 kg/m^3, similar to the bulk density of the dense bed (1560 kg/m^3), so the object could be considered to have a neutrally-buoyant behavior. The position of the object was determined experimentally using digital image analysis and the trajectories in the rising and sinking processes were obtained. For the rising process, it was observed that the object was more prone to rise at the middle of the bed, and concerning the sinking process, it was observed that the object sank with more probability by the sides of the bed. This is in accordance with the preferential paths of rising bubbles and sinking dense phase observed by other authors. The velocity of the object was also calculated from the trajectories, obtaining a sinking velocity comparable with the sinking velocity of the dense phase. The dense phase velocity was estimated using the Kunii and Levenspiel correlation (Kunii & Levenspiel, 1991) presented in equation (1.1). The rising object velocity was obtained, and compared to the mean bubble velocity calculated by the Davidson & Harrison (1963) correlation showed in equation (1.2) using the Shen correlation (Shen *et al.*, 2004) presented in equation (1.3) to obtain the bubble diameter for 2-D beds.

$$v_{dp} = \frac{f_w \delta U_B}{1 - \delta - f_w \delta} \tag{1.1}$$

$$U_B = U - U_{mf} + \Phi \sqrt{g D_B} \tag{1.2}$$

$$D_B = \left[\left(\frac{8(2^{3/4} - 1)}{\lambda} \right) (U - U_{mf}) \left(h_{fb} + \frac{\lambda}{\pi (2^{3/4} - 1)} \frac{A_0}{T} \right) \right]^{2/3} g^{-1/3} \tag{1.3}$$

where v_{dp} is the downwards velocity of the dense phase and depends on the bubble wake fraction, f_w, the bubble fraction in the bed, δ, and the bubble velocity, U_B. The bubble diameter, D_B, is a function of the gas velocity, U, the minimum fluidization velocity, U_{mf}, the fixed bed height, h_{fb}, the area of the distributor per number of orifices, A_0, the bed thickness, T, and the gravity, g. Finally, λ and Φ are constants determined experimentally.

Both the mean rising and sinking velocities of the object obtained experimentally are plotted in Figure 1.1 together with the bubble velocity and dense phase downwards velocity, estimated by the respective correlations, for different dimensionless gas velocities, U/U_{mf}.

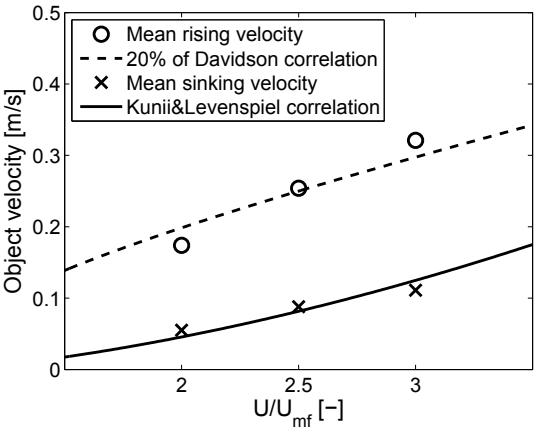

Figure 1.1: Object rising and sinking velocities (taken from Soria-Verdugo *et al.* (2011*b*)).

The object velocity in the sinking path is similar to the dense phase downwards velocity. On the other hand, the rising process of an object immersed in the bed is characterized by an ascension velocity of 20% the mean bubble velocity, as it is observed in Figure 1.1. These results are quite in accordance to the literature as previously stated.

In the rising process, the object was not always lifted to the bed surface by a single bubble, but the rising motion was composed of the combined effect of several passing bubbles. Such a motion can be represented by a series of jumps or jerks, as described by Rios *et al.* (1986). This phenomenon was characterized by Soria-Verdugo *et al.* (2011*b*). They observed that the object can be lifted to the bed surface by a single bubble or with a number of jumps in a cycle. A cycle is here defined between the instant when the object starts the sinking path at the bed surface, and the instant when, after completing its motion inside the dense bed, it reaches back to the surface. The relative frequency of the object to reach the surface by the action of a single bubble or by a determined number of bubbles in a cycle is plotted in Figure 1.2.

The probability of finding a low number of jumps in the rising process is higher than finding cycles composed of a high number of jumps, as can be observed in Figure 1.2. The experimental results showed a decrease of the relative frequency with the number of jumps, given by a geometrical equation represented in the form of a probability density function, $P\left(N_{jumps}\right)$, in

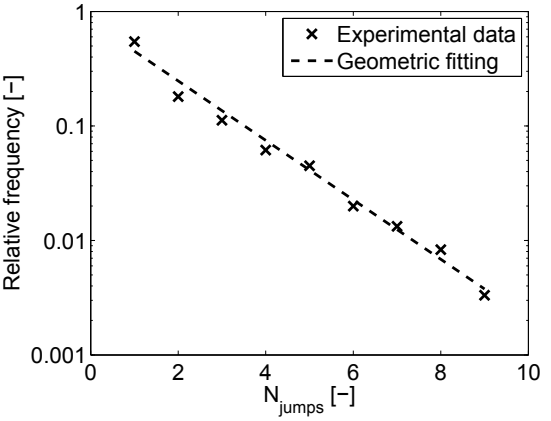

Figure 1.2: Relative frequency of number of jumps needed by the object to get the surface in a cycle (taken from Soria-Verdugo *et al.* (2011*b*)).

equation (1.4).

$$P(N_{jumps}) = p(1-p)^{N_j-1} \text{ for } N_{jumps} = 1, 2, 3... \tag{1.4}$$

where N_{jumps} is the number of jumps in a cycle. The value of p in the fitting obtained to match with the experimental data was 0.45. The fitting is plotted also in Figure 1.2 for $p = 0.45$. This value of p means that the object has an average probability of 45% to get directly the bed surface by the action of a single bubble, and thus a complementary probability, $(1-p)$, of 55% of detaching from the bubble during the rising path. In Figure 1.2 only the experimental data obtained by an object with a neutrally-buoyant behavior was plotted. The same value of p was obtained for different object characteristics and operational conditions in a second work (Soria-Verdugo *et al.*, 2011*a*). In that work, the object was varied in size and density, provided that the object moved throughout the bed with a proper circulation. Furthermore, the fixed bed height, the dimensionless gas velocity and the particle diameter of the dense phase was modified and the same average value of p was also obtained. When the buoyancy forces are predominant and the circulation is poor, objects remaining close to the bed surface or sinking to the distributor and remaining there, the parameter has no longer meaning. Note that varying the dimensionless gas velocity and the bed height suppose a variation of the bubble diameter, but no effect was found on the value of the parameter p. Therefore, it can be concluded that an object with a proper circulation has an average probability of 45% in the whole bed to reach the bed surface directly when attaching to a single bubble.

Finally, the maximum depth attained by an object in a cycle was studied. The relative frequency of an object with a neutrally-buoyant behavior to attain a maximum depth is plotted in Figure 1.3 for the experimental data. The maximum depth attained, d_m, is presented in dimensionless form, divided by the fixed bed height, h_{fb}, being 0 at the surface of the bed and 1 at the bottom. The maximum depth attained was found to follow a parabolic law, with minimum probability found for medium depths as can be observed in Figure 1.3.

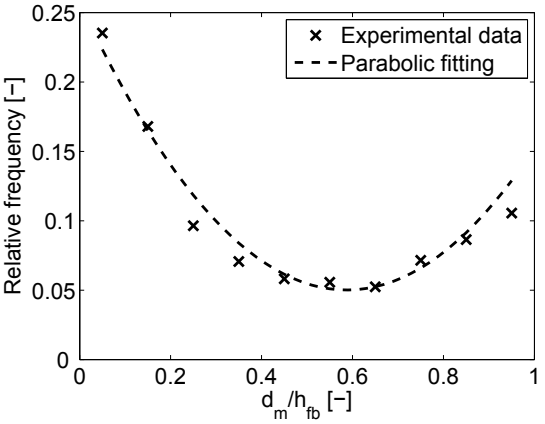

Figure 1.3: Probability of the object to attain a maximum depth in a cycle (taken from Soria-Verdugo *et al.* (2011*b*)).

1.3 Application to fuel conversion processes

The lateral and vertical motion, the residence time in the bed, and the thermal conversion rate of the fuel particles are main parameters for the design of fluidized bed reactors (Gómez-Barea & Leckner, 2010). As stated in section 1.1, fluidized beds are characterized by a high vertical mixing due to the action of bubbles, thus the lateral mixing is the limiting factor in these applications. The Damköhler number, Da, is defined, for horizontal processes, as the ratio of the lateral transport time to the thermal conversion time of a fuel particle (Leckner *et al.*, 2011), and is given in equation (1.5). For high Damköhler numbers ($Da >> 1$) the conversion process dominates and the thermal conversion of the fuel particle occurs close to the feeding port. On the other hand, for low Damköhler numbers ($Da << 1$), the lateral motion is faster than the thermal conversion process, producing a better distribution of fuel particles throughout

the bed.

$$Da = \frac{\tau_{trans}}{\tau_{conv}} \tag{1.5}$$

where τ_{trans} is the lateral transport time and τ_{conv} is the thermal conversion time.

The lateral motion of a fuel particle can be described by the lateral dispersion coefficient. Several authors have determined experimentally the lateral dispersion coefficient in both 2-D and 3-D fluidized beds, using different techniques, and obtaining values in a wide range between $3 \cdot 10^{-4}$ and 0.14 m^2/s, as reviewed by Olsson *et al.* (2012). For 2-D beds, Salam *et al.* (1987) and Xiao *et al.* (1998) employed solids concentration sampling to obtain the lateral dispersion coefficient, whereas Pallarès & Johnsson (2006) used a tracking technique of fuel particles. In 3-D beds, defluidized bed sieving and residence time distribution were employed by Xiang *et al.* (1987) and Bi *et al.* (1995) respectively. Olsson *et al.* (2012) obtained the lateral dispersion coefficient experimentally in a large-scale 3-D bubbling fluidized bed using a tracking technique of the fuel motion in the freeboard and in the surface of the bed, for different gas velocities.

On the other hand, the thermal conversion processes during the lateral motion of the fuel particle in the bed can be characterized distinguishing two main reactions: devolatilization of the fuel and char combustion (Leckner & Werther, 2000). The lower reaction time corresponds to devolatilization processes. The devolatilization time has been measured in the literature as a function of the fuel particle size and shape, obtaining values between 20 and 350 seconds (de Diego *et al.*, 2002; Wang *et al.*, 2005; Sreekanth *et al.*, 2008).

There are basically two alternatives to feed the fuel in a fluidized bed reactor: the freeboard or inside the dense bed. The former case was characterized by its simplicity and the economical manufacturing of the feeding ports compared with locating the feeding ports inside the dense bed. Depending on the devolatilization process, some possible situations can occur in relation to the vertical location of the feeding ports: i) the fuel particle stays floating at the surface of the bed most of the time of the devolatilization process; ii) the fuel particle remains at the bottom of the bed during the devolatilization process; or iii) the fuel particle moves properly from the bottom to the surface of the bed while the devolatilization takes place (Fiorentino *et al.*, 1997; Gómez-Barea & Leckner, 2010). In addition, the horizontal distribution over the cross section

of the fluidized bed reactor is an important issue for a proper distribution of the fuel throughout the bed.

1.4 Scope of the thesis

This PhD thesis presents experimental work and modeling concerning the motion of large objects in a fluidized bed. Most of the experiments were carried out in a 2-D bubbling fluidzed bed, but a 3-D lab-scale fluidized bed was also used to compare and extrapolate some results obtained from the 2-D tests. In both facilities, the behavior of the object was characterized with a measurement technique based on digital image analysis. On the other hand, the model proposed employed as inputs the results obtained in tests made in this PhD thesis and in the literature. The model also required the simulation of several statistical variables, which were performed using Monte Carlo methods.

The PhD thesis has been divided in six chapters. In Chapter 2 the experimental facilities employed in the experiments were described. From Chapter 3 to Chapter 5 the core of the PhD thesis is presented in the form of three independent articles with their introduction, notation, references and conclusions.

The 2-D and 3-D facilities and the measurement technique employed in the experiments were described in detail in Chapter 2. The measurement technique consisted of two different methods of tracking the object in the 2-D bubbling fluidized bed. The motion of the object, either when it is immersed in the bed or when it is in the freeboard, was characterized using digital image analysis. For the 3-D experiments, only the presence of the object in the surface was assessed.

In Chapter 3, the object motion in the freeboard was analyzed experimentally in a 2-D bubbling fluidized bed. The object ejection was characterized for several gas velocities and related to bubble parameters. The time spent by the object in the freeboard and its lateral displacement were also measured. Finally, the motion in the freeboard was modeled, based on the ballistic equations. The inputs of the model were the statistical distributions of the characteristic parameters for the object ejection obtained during the experiments. These statistic variables were simulated employing a Monte Carlo method. Therefore, the lateral displacement and the time of flight were calculated and compared with the experimental results.

In Chapter 4, the vertical object motion when it is immersed in a 2-D bubbling fluidized bed was modeled. The model was based on experimental

data, some made in this PhD thesis, other from the previous works and from well-known correlations of the literature. A Monte Carlo method was employed to simulate the relations between the statistical variables that represent the object rising and sinking processes. The time that an object spent to complete a cycle and the maximum depth attained in this cycle were calculated and compared to experimental results. An extrapolation of the 2-D results to a lab-scale 3-D fluidized bed was also made and validated.

The last main chapter of this PhD thesis, Chapter 5, focused on the motion of a fuel particle in a large-scale fluidized bed. The motion was modeled employing the statistical parameters obtained experimentally in Chapter 3 and Chapter 4. The model was completed including new variables from the literature for several aspects that were not characterized in previous sub-models. The representative variables of the different processes were simulated with a global Monte Carlo method and validated with an experimental work presented in the literature. The lateral displacement of the fuel particle and the time employed by a fuel particle to complete its motion in the fluidized bed were determined. As a particular application, the location of the feeding ports were optimized to ensure a proper distribution of the fuel particle throughout the whole bed.

Finally, the conclusions obtained in this PhD thesis were summarized in Chapter 6.

Notation

A_0	Area of the distributor per number of orifices [m^2]
Da	Damköhler number [−]
D_B	Bubble diameter [m]
d_m	Maximum depth attained by the object [m]
f_w	Bubble wake fraction [−]
g	Gravity [$m{\cdot}s^{-2}$]
N_{jumps}	Number of jumps in a cycle [−]
h_{fb}	Fixed bed height [m]
p	Probability of an object to get the bed surface by the action of a single bubble [−]
$P\left(N_{jumps}\right)$	Probability density function of the number of jumps [−]
T	Bed thickness [m]
U	Superficial gas velocity [$m{\cdot}s^{-1}$]
U_B	Bubble velocity [$m{\cdot}s^{-1}$]

U_{mf}	Minimum fluidization velocity [m·s^{-1}]
v_{dp}	Downwards velocity of the dense phase [m·s^{-1}]
δ	Bubble fraction in the bed [–]
λ	Constant determined experimentally [–]
Φ	Constant determined experimentally [–]
τ_{conv}	Thermal conversion time [s]
τ_{trans}	Lateral transport time [s]

References

Bai, W., Keller, N.K.G., Heindel, T.J. & Fox, R.O. 2013 Numerical study of mixing and segregation in a biomass fluidized bed. *Powder Technology* 237 (0), 355 – 366.

Bi, J., Yang, G. & Kojima, T. 1995 Lateral mixing of coarse particles in fluidized beds of fine particles. *Chemical Engineering Research and Design* 73, 162–167.

Bruni, G., Solimene, R., Marzocchella, A., Salatino, P., Yates, J.G., Lettieri, P. & Fiorentino, M. 2002 Self-segregation of high-volatile fuel particles during devolatilization in a fluidized bed reactor. *Powder Technology* 128 (1), 11 – 21.

Davidson, J.F. & Harrison, D. 1963 *Fluidised particles*, 1st edn. Cambridge: Cambridge University Press.

de Diego, L.F., García-Labiano, F., Abad, A., Gayán, P. & Adánez, J. 2002 Modeling of the devolatilization of nonspherical wet pine wood particles in fluidized beds. *Industrial & Engineering Chemistry Research* 41 (15), 3642 – 3650.

Fiorentino, M., Marzocchella, A. & Salatino, P. 1997 Segregation of fuel particles and volatile matter during devolatilization in a fluidized bed reactor-II. Experimental. *Chemical Engineering Science* 52 (12), 1909 – 1922.

Gómez-Barea, A. & Leckner, B. 2010 Modeling of biomass gasification in fluidized bed. *Progress in Energy and Combustion Science* 36 (4), 444 – 509.

Ito, O., Kawabe, R., Miyamoto, T., Orita, H., Mizumoto, M., Miyadera, H., Tomuro, J., Hokari, N. & Iwase, T. 1999 Direct mea-

surement of particle motion in a large-scale FBC boiler model. In *International Conference on Fluidized Bed Combustion*, p. 217.

Kunii, D. & Levenspiel, O. 1991 *Fluidization Engineering*, 2nd edn. Boston: Butterworth-Heinemann.

Leckner, B., Szentannai, P. & Winter, F. 2011 Scale-up of fluidized-bed combustion - a review. *Fuel* 90 (10), 2951 – 2964.

Leckner, B. & Werther, J. 2000 Scale-up of circulating fluidized bed combustion. *Energy & Fuels* 14 (6), 1286 – 1292.

Lim, K.S. & Agarwal, P.K. 1994 Circulatory motion of a large and lighter sphere in a bubbling fluidized bed of smaller and heavier particles. *Chemical Engineering Science* 49 (3), 421 – 424.

Nguyen, T.H. & Grace, J.R. 1978 Forces on objects immersed in fluidized beds. *Powder Technology* 19 (2), 255 – 264.

Nienow, A.W., Rowe, P.N. & Chiba, T. 1978 Mixing and segregation of a small portion of large particles in gas fluidized beds of considerably smaller ones. *AIChe Symposium Series* 74, 45 – 53.

Olsson, J., Pallarès, D. & Johnsson, F. 2012 Lateral fuel dispersion in a large-scale bubbling fluidized bed. *Chemical Engineering Science* 74 (0), 148 – 159.

Pallarès, D., Díez, P & Johnsson, F. 2007 Experimental analysis of fuel mixing patterns in a fluidized bed. In *The 12th International Conference on Fluidization - New Horizons in Fluidization Engineering*, pp. 929 – 936.

Pallarès, D. & Johnsson, F. 2006 A novel technique for particle tracking in cold 2-dimensional fluidized beds - simulating fuel dispersion. *Chemical Engineering Science* 61 (8), 2710 – 2720.

Rees, A.C., Davidson, J.F., Dennis, J.S. & Hayhurst, A.N. 2005 The rise of a buoyant sphere in a gas-fluidized bed. *Chemical Engineering Science* 60 (4), 1143 – 1153.

Rios, G. M., Dang Tran, K. & Masson, H. 1986 Free object motion in a gas fluidized bed. *Chemical Engineering Communications* 47 (4-6), 247 – 272.

Salam, T.F., Ren, Y. & Gibbs, B.M. 1987 Lateral solid and thermal dispersion in fluidized bed combustors. In *9th International Conference on Fluidized Bed Combustion*, pp. 541 – 545.

Shen, L., Johnsson, F. & Leckner, B. 2004 Digital image analysis of hydrodynamics two-dimensional bubbling fluidized beds. *Chemical Engineering Science* 59 (13), 2607 – 2617.

Soria-Verdugo, A., Garcia-Gutierrez, L.M., García-Hernando, N. & Ruiz-Rivas, U. 2011*a* Buoyancy effects on objects moving in a bubbling fluidized bed. *Chemical Engineering Science* 66 (12), 2833 – 2841.

Soria-Verdugo, A., Garcia-Gutierrez, L.M., Sánchez-Delgado, S. & Ruiz-Rivas, U. 2011*b* Circulation of an object immersed in a bubbling fluidized bed. *Chemical Engineering Science* 66 (1), 78 – 87.

Soria-Verdugo, A., García-Hernando, N., Almendros-Ibáñez, J.A. & Ruiz-Rivas, U. 2011*c* Motion of a large object in a bubbling fluidized bed with a rotating distributor. *Chemical Engineering and Processing: Process Intensification* 50 (8), 859 – 868.

Sreekanth, M., Sudhakar, D.R., Prasad, B.V.S., Kolar, A.K. & Leckner, B. 2008 Modelling and experimental investigation of devolatilizing wood in a fluidized bed combustor. *Fuel* 87 (12), 2698 – 2712.

Wang, X., Kersten, S.R.A., Prins, W. & van Swaaij, W.P.M. 2005 Biomass pyrolysis in a fluidized bed reactor. part 2: Experimental validation of model results. *Industrial & Engineering Chemistry Research* 44 (23), 8786 – 8795.

Wirsum, M., Fett, F., Iwanowa, N. & Lukjanow, G. 2001 Particle mixing in bubbling fluidized beds of binary particle systems. *Powder Technology* 120, 63 – 69.

Xiang, Q., Huang, G., Ni, M., Cen, K. & Tao, T. 1987 Lateral dispersion of large coal particles in an industrial scale fluidised bed combustor. In *9th International Conference on Fluidized Bed Combustion*, pp. 546 – 553.

Xiao, P., Yan, G. & Wang, D. 1998 Investigation on horizontal mixing of particles in dense bed in circulating fluidized bed (CFB). *Journal of Thermal Science* 7 (2), 78 – 84.

Zhang, Y., Jin, B. & Zhong, W. 2009 Experimental investigation on mixing and segregation behavior of biomass particle in fluidized bed. *Chemical Engineering and Processing: Process Intensification* 48 (3), 745 – 754.

CHAPTER
TWO

Experimental setup and measurement technique

Contents

The experiments presented in this PhD thesis were carried out in two different facilities. Most of the tests were performed in a 2-D bubbling fluidized bed, while a lab-scale 3-D bubbling fluidized bed was used to validate the extrapolation of some results obtained in the 2-D facility.

2.1 2-D facility

The experimental facility consisted of a 2-D bubbling fluidized bed with a height of 2 m and a width of 0.5 m. The front of the bed was made of glass, allowing optical access. The rear wall was made of aluminum, and it was covered with a black paper to obtain a higher contrast between the dense phase (white) and the bubbles (black). The fluidization gas was air, supplied from a compressor, and conducted to the plenum chamber by two air inlets to guarantee a proper distribution. The thickness of the facility, T, was 0.005 m and 0.010 m in two different sets of experiments. For the tests employing a thickness of 0.005 m, two different fixed bed heights, h_{fb}, of 0.3 m and 0.5 m were used. The minimum fluidization velocity, U_{mf}, was measured to be 0.43 m/s and 0.49 m/s for the

two fixed bed heights respectively. On the other hand, in the experiments carried out with the thickness of 0.010 m, the fixed bed height employed was 0.5 m and the minimum fluidization velocity was 0.32 m/s. The differences of the minimum fluidization velocity between different thickness and bed heights were due to the wall effects in a 2-D geometry. Several authors have studied the influence of walls on the minimum fluidization velocity, modifying the bed thickness, bed height and the size and density of the bed material (Geldart & Cranfield, 1972; Caicedo *et al.*, 2002; Sánchez-Delgado *et al.*, 2011, 2013). The general agreement, for different bed characteristics, is that there is an increment of the minimum fluidization velocity with the fixed bed height and a decrease when the bed thickness increases. This is in accordance with the results presented in this PhD thesis. An scheme of the 2-D facility can be observed in Figure 2.1.

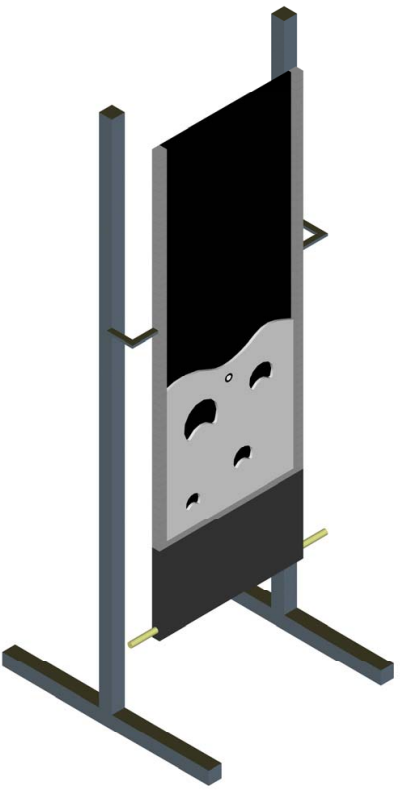

Figure 2.1: Scheme of the experimental 2-D facility.

The bed material used in all the experiments of this PhD thesis was glass spheres, ballotini particles, with a diameter in the range $600 - 800$ μm. The density of the dense phase particle was 2500 kg/m^3, corresponding to type B of the Geldart's classification (Geldart, 1973) and the bulk density of the bed was measured to be 1560 kg/m^3 according to *UNE-CEN/TS 15103 EX*. As a result, the value of the bed void fraction was 0.38. An image of the bed material, obtained with an electronic microscopic is showed in Figure 2.2.

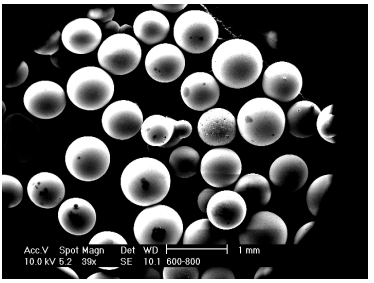

Figure 2.2: Ballotini particles observed with an electronic microscope.

The air distributor was built in aluminum and consisted of a plate with orifices of diameter, d_o, equal to 0.001 m. The dimensions of the distributor and the configuration of the holes in the plate were different for the two bed thickness employed in the experiments. For the thickness of 0.005 m the distributor plate was composed of a row of orifices with a separation between holes, $d_1 = 0.010$ m, while for the bed thickness of 0.010 m the orifices were distributed in a triangular configuration composed of two rows separated a distance, $s = 0.0033$ m. A scheme of the air distributors used in the different experiments is showed in Figure 2.3.

The variation of the pressure drop of the distributor, ΔP_{dist}, with the gas velocity, U, was measured. Fitting curves of the experimental data are plotted in Figure 2.4 for the two different thicknesses of the distributor plates. The distributor pressure drop is higher than 30% the bed pressure drop in all experimental cases. Therefore, the pressure drop for each distributor was sufficient to ensure a homogeneous distribution of the air throughout the bed width according to Karri & Werther (2003).

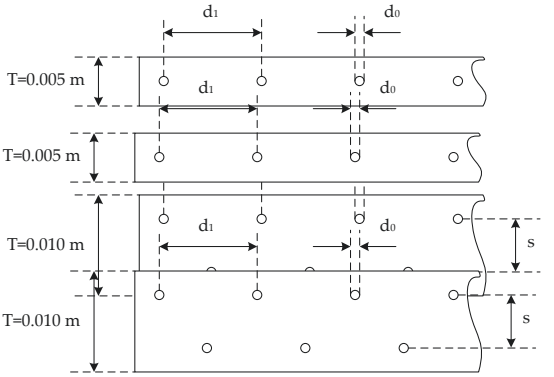

(b)

Figure 2.3: Scheme of the distributor plates with thicknesses of (a) 0.005 m and (b) 0.010 m.

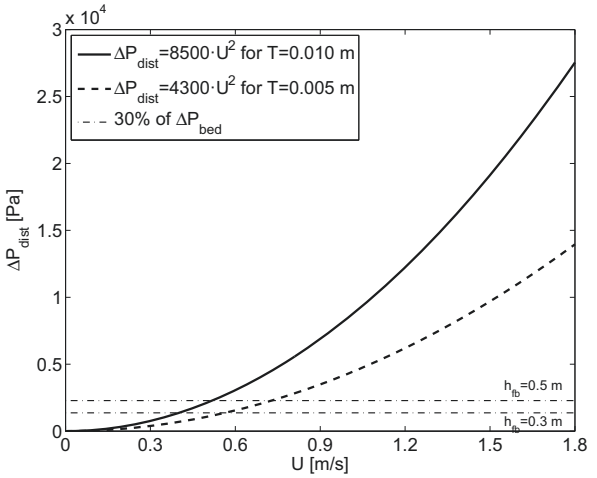

Figure 2.4: Pressure drop of the two different distributor plates used in the 2-D facility.

2.2 3-D facility

The 3-D experimental facility was a lab-scale bubbling fluidized bed. It consisted of a cylindrical vessel with an inner diameter of 0.192 m, and a height of 1 m. The fixed bed height was kept constant in all experiments, with a value of 0.192 m (aspect ratio equal to unity). The fluidization gas used was also air. The minimum fluidization velocity was 0.25 m/s, using the same bed material

employed in the experiments of the 2-D facility. A scheme of the 3-D facility is shown in Figure 2.5.

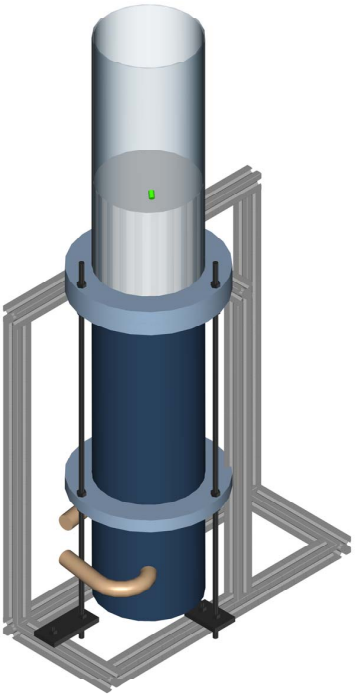

Figure 2.5: Scheme of the experimental 3-D facility.

The distributor was designed in order to guarantee the uniform and homogeneous fluidization across the whole bed, minimizing the de-fluidized zones over the distributor according to Geldart & Baeyens (1985), Kunii & Levenspiel (1991) and Karri & Werther (2003). Therefore, a perforated plate with a thickness of 0.006 m was selected, with 275 holes of diameter, $d_h = 0.002$ m. The holes were distributed in a triangular mesh with a pitch of $L_h = 0.011$ m. A scheme of the perforated plate is shown in Figure 2.6. A deeper study of this distributor plate is presented in Soria-Verdugo (2010).

The pressure drop of the distributor plate is plotted in Figure 2.7 as a function of the dimensionless gas velocity, U/U_{mf}. The distributor pressure drop is higher than 30% the bed pressure drop. Therefore, homogeneous fluidization was ensure according to Karri & Werther (2003) for all of the dimensionless gas velocities employed in the experiments of the 3-D facility, as can be observed in Figure 2.7.

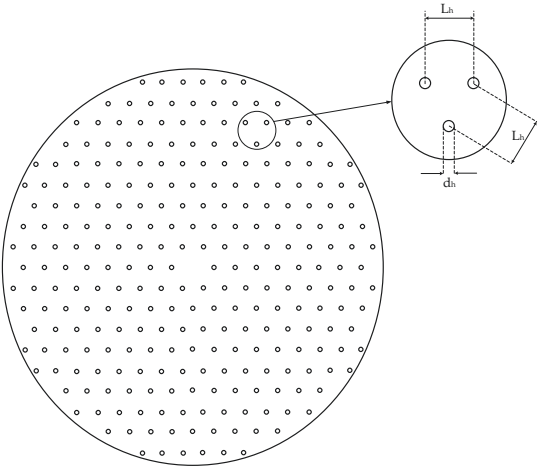

Figure 2.6: Scheme of the distributor plate used in the 3-D facility.

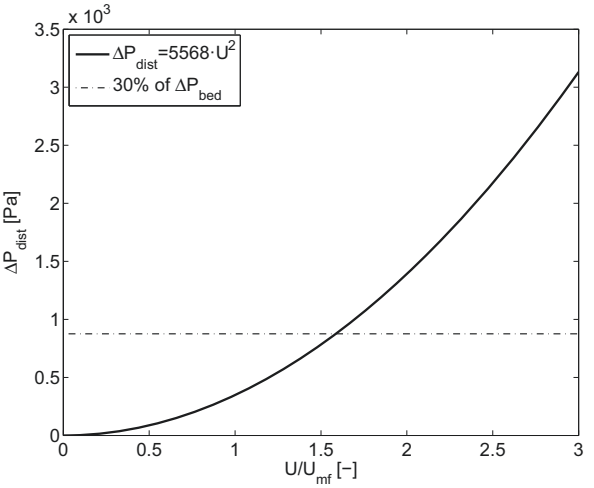

Figure 2.7: Pressure drop of the distributor plate employed in the 3-D facility.

2.3 Measurement technique

The aim of this PhD thesis is to study the behavior of objects in bubbling fluidized beds. Therefore, the development of a measurement technique to track the object, based on digital image analysis, is mandatory. In fact, three different tracking techniques were developed and employed, to obtain different information concerning the object motion, and for application in either 2-D or 3-D facilities. A frontal point of view of the acquisition system was employed

for the tests carried out in the 2-D facility. On the other hand, for the 3-D experiments a zenith point of view was used.

Two different measurement techniques were used in the 2-D experiments. The first measurement technique can just characterize the object motion, while in the second, the object motion can be characterized together with the dense phase and the bubbles.

2.3.1 Object tracking in darkness in the 2-D facility

A measurement technique based on digital image analysis, was used to obtain the position and the velocity of an object when it is immersed in a 2-D bed. The object used during these tests was a biomass pellet of cylindrical shape with a diameter of 0.0064 m and a length equal to 0.019 m. During these experiments the bed thickness was 0.010 m. The object density was measured to be 1508 kg/m^3, a similar value to the bulk density of the bed material (1560 kg/m^3). The object could be considered as a neutrally-buoyant object, showing a proper circulation throughout the bed (Soria-Verdugo *et al.*, 2011*b*). The motion of the object throughout the bed was recorded with a standard camera (*Nikon D80 10.6Mpx*) with an acquisition frequency of 1.4 and 30 fps. The measurements were carried out in complete darkness. The object was covered with strontium aluminate, emitting a phosphorescent green light that allowed its identification. A picture of the cylindrical object is showed in Figure 2.8.

Figure 2.8: Object used in the experiments in complete darkness.

The first image of each serial was taken with light in order to determine the bed limits. The object identification was carried out employing a threshold and binarizing the image, transforming the green color of the object to white. The center of mass of the object was calculated, and thus the position of the object at each instant was determined. A scheme of the process followed in the characterization of the position of the object is showed in Figure 2.9.

The image of the object inside the dense bed taken with light is presented in Figure 2.9(a). The object location is not easy to asses, but it is pointed out

with a circle in this figure. The bed limits can be defined and thus the position of the object in the bed can be determined. The image in darkness is showed in Figure 2.9(b) with the object emitting green light, obtaining a high contrast. Finally, the picture binarized can be observed in Figure 2.9(c), and the center of mass is marked with a red cross. Therefore, the position of the object was characterized with high accuracy at each instant of its motion.

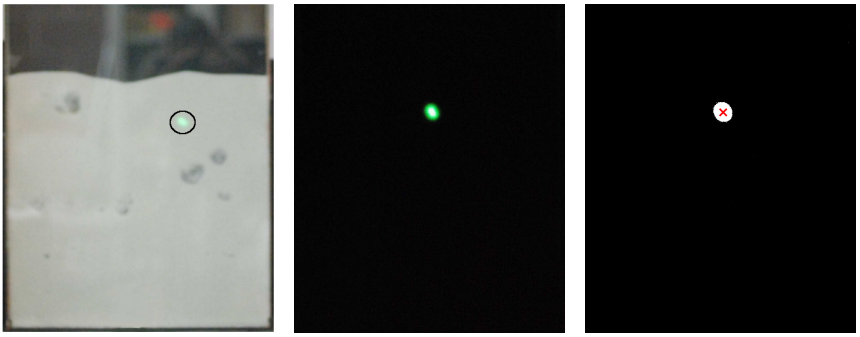

(a) (b) (c)

Figure 2.9: Processes followed to detect the object; (a) with light to identify the bed limits, (b) image taken in darkness and (c) image binarized showing its center of mass.

The position of the object was determined with an acquisition frequency of 1.4 fps, but the trajectory and thus the velocity of the object were determined employing the same procedure but using an acquisition frequency of 30 fps in order to obtain the path followed by the object more accurately. As an example of the results obtained from the tracking technique using 30 fps, the trajectory followed by the object in the bed is plotted in Figure 2.10 over the lighted image. The velocity of the object, both in the sinking and in the rising path, were determined from these experiments. The measurement technique presented in this section was developed using an algorithm implemented in Matlab®. The results obtained from this technique are presented in Chapter 4.

2.3.2 Object tracking with light in the 2-D facility

The aim of this measurement technique was the characterization of the dense phase, the bubbles and the object at the same time, for the determination of the object behavior when it is ejected by the bubbles into the freeboard. The object used in this tests had a disc shape, with a diameter of 0.02 m and a thickness

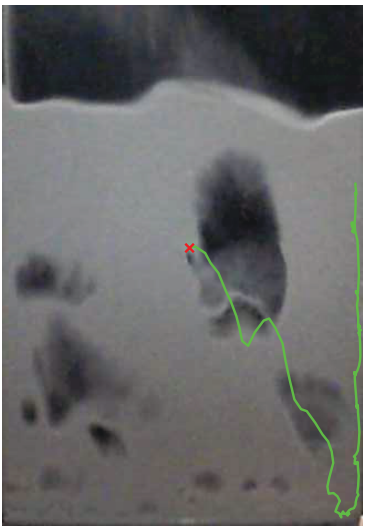

Figure 2.10: Trajectory of the object in the bed depicted over the lighted image.

of 0.003 m. During these experiments the bed thickness was 0.005 m. The object was made with a black ribbon in order to differentiate from the white dense phase and with a white circle in its center used for contrasting with the bubbles and freeboard (black rear wall). Therefore, the object motion can be characterized when it is immersed in the dense bed and when it is moving in the freeboard or inside a bubble. The density of the object was selected to be 1200 kg/m^3 and thus the behavior of the object in the bed was flotsam for low gas velocities, $U/U_{mf} < 2.5$, spending more than 75% of the time in the upper half of the bed. Nevertheless, this object shows a neutrally-buoyant behavior for higher velocities, $U/U_{mf} \geq 2.5$, presenting a proper circulation in the whole bed. Therefore, two different behaviors can be studied using this object as a function of U/U_{mf}. A picture of the object used is showed in Figure 2.11.

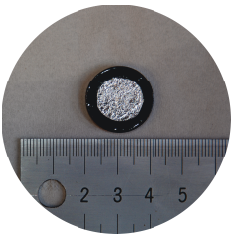

Figure 2.11: Object used in the experiments with light.

The acquisition system consisted of a high speed video camera, *Redlake Motion pro X3 4Gb*, and an illumination system. The illumination was carried out with four spotlights of 650 W, giving a homogeneous illumination of the whole bed. The acquisition frequency employed was 125 fps. The tracking of the object was performed employing a rectangular window centered in the object. A threshold and a binarization were applied over the tracking window in order to distinguish the object and to calculate the center of mass, and thus the position of the object throughout the bed can be obtained at each instant. The dimensions of the rectangular window were selected according to the object velocities calculated in previous works reviewed in section 1.1.

As stated above, the object was designed with a black ribbon in order to differentiate it from the dense phase and with a white circle to be distinguish from the bubbles and the freeboard. In Figure 2.12 the real image recorded by the camera and the binary image applying the threshold are plotted. As can be observed in Figure 2.12(a),(b), the black ribbon of the object allow the detection when it is immersed in the dense bed. On the other hand, when the object is in the freeboard, the white circle allows the detection during its motion, as can be seen in Figure 2.12(c),(d) for the real and binarized image. The center of mass of the object is marked in the binary images with a red cross. Therefore, the ejection of the object and its motion in the freeboard can be characterized properly using this measurement technique. The measurement technique presented in this section was developed using an algorithm implemented in Matlab®. The results obtained from this technique are presented in Chapter 3.

2.3.3 Object detection on the bed surface of the 3-D facility

The 3-D facility was employed to determine the time spent by an object with a proper circulation inside the 3-D fluidized dense bed.

The experiments carried out in the 3-D facility consisted of zenith recordings of the surface of the fluidized bed. The object could only be detected while it is in the freeboard. The measurements were made in complete darkness and the object used was the biomass pellet covered with strontium aluminate described in section 2.3.1. The object was detected correctly for dimensionless gas velocities lower than 3. For $U/U_{mf} \geq 3$, an accurate identification of the object in the freeboard was not possible due to the vigorous splashing of the bubbles. The acquisition system was a standard camera with a frequency of

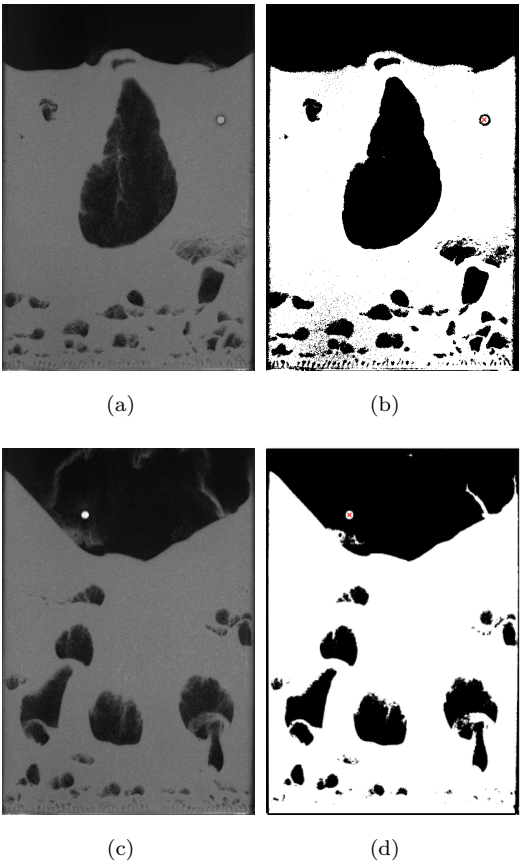

(a) (b)

(c) (d)

Figure 2.12: Differentiation of the object (a) in a real image inside the dense bed, (b) in the binary image inside the dense bed, (c) in a real image in the freeboard and (d) in the binary image in the freeboard.

30 fps. The procedure followed to determine the position of the object in the surface was the same than that employed in section 2.3.1. A threshold was applied to binarize the image and calculate the position of the object in the freeboard of the bed. This procedure is schematized in Figure 2.13, where the image recorded in darkness with the object emitting in green light (Figure 2.13(a)) is plotted, together with the binary image obtained after the application of the threshold (Figure 2.13(b)). The position of the center of mass of the object is marked with a red cross. These results are also presented in Chapter 4.

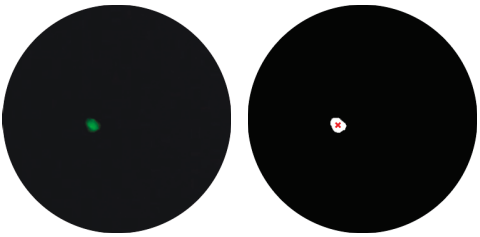

(a) (b)

Figure 2.13: Different processes in the detection of the object in the 3-D facility; (a) in darkness and (b) in the binary image.

References

Caicedo, G.R., Ruiz, M.G., Marqués, J.P. & Soler, J.G. 2002 Minimum fluidization velocities for gas-solid 2D beds. *Chemical Engineering and Processing: Process Intensification* 41 (9), 761 – 764.

Geldart, D. 1973 Types of gas fluidization. *Powder Technology* 7 (5), 285 – 292.

Geldart, D. & Baeyens, J. 1985 The design of distributors for gas-fluidized beds. *Powder Technology* 42 (1), 67 – 78.

Geldart, D. & Cranfield, R.R. 1972 The gas fluidisation of large particles. *The Chemical Engineering Journal* 3 (0), 211 – 231.

Karri, S.B.R. & Werther, J. 2003 *Handbook of fluidization and fluid-particle systems*. New York: Marcel Dekker Inc.

Kunii, D. & Levenspiel, O. 1991 *Fluidization Engineering*, 2nd edn. Boston: Butterworth-Heinemann.

Sánchez-Delgado, S., Almendros-Ibáñez, J.A., García-Hernando, N. & Santana, D. 2011 On the minimum fluidization velocity in 2D fluidized beds. *Powder Technology* 207, 145 – 153.

Sánchez-Delgado, S., Marugán-Cruz, C., Soria-Verdugo, A. & Santana, D. 2013 Estimation and experimental validation of the circulation time in a 2D gas-solid fluidized beds. *Powder Technology* 235, 669 – 676.

Soria-Verdugo, A. 2010 Motion of objects immersed in a bubbling fluidized bed. PhD thesis, Carlos III University of Madrid.

Soria-Verdugo, A., Garcia-Gutierrez, L.M., García-Hernando, N. & Ruiz-Rivas, U. 2011*a* Buoyancy effects on objects moving in a bubbling fluidized bed. *Chemical Engineering Science* 66 (12), 2833 – 2841.

Soria-Verdugo, A., Garcia-Gutierrez, L.M., Sánchez-Delgado, S. & Ruiz-Rivas, U. 2011*b* Circulation of an object immersed in a bubbling fluidized bed. *Chemical Engineering Science* 66 (1), 78 – 87.

CHAPTER
THREE

Study of the object motion in the freeboard of a bubbling fluidized bed

Contents

3.1 Introduction

The motion of a large non-reacting object in the freeboard of a bubbling fluidized bed was experimentally characterized and compared with Monte Carlo simulations. The tracking technique based on digital image analysis presented in section 2.3.2 was used to study the object motion, both when it is immersed in the dense bed and in the freeboard. A model, based on the kinematic equations of the motion, and relying on a minimum set of experimental data, was used to obtain the relevant characteristics of the process. The relation between the statistical distributions of experimental data was simulated using a Monte Carlo method.

The object motion in the freeboard was observed to be only affected by gravity and it could be described as a ballistic motion, characterized by the initial velocity of the object, or ejection velocity. The ejection velocity modulus and angle were experimentally determined for several bed conditions, varying the gas velocity and the bed height. The results showed a good agreement between the mean values of the ejection velocity and the mean bubble velocity for all conditions. Probability distributions for the modulus and angle of the ejection velocity were obtained from the experimental measurements.

The object lateral displacement and the time of flight of the object in the freeboard were calculated using three parallel approaches, with different degrees of simplicity and accuracy, employing the Monte Carlo model. The results of the model were compared to the experimental results.

3.2 Experimental procedure

3.2.1 Experimental setup

A detailed description of the experimental facility and the measurement technique employed in these tests can be found in sections 2.1 and 2.3.2 respectively. In this section, just a brief description is presented.

The experimental tests described in this chapter were carried out in the 2-D facility with a thickness of 0.005 m and the object used was that with a disc shape and density of 1200 kg/m^3. The experiments were performed for two different fixed bed heights, 0.3 m and 0.5 m. Four values of the dimensionless gas velocity, U/U_{mf}, for each fixed bed height were employed: 1.8, 2.3, 2.8 and 3.4 for a fixed bed height of 0.3 m and 1.6, 2, 2.5 and 3 for a fixed bed height of 0.5 m, obtaining a total of eight different experimental cases. The bed material was ballotini particles with a bulk density of 1560 kg/m^3 so that the object had a flotsam behavior for low dimensionless gas velocities ($U/U_{mf} < 2.5$), while for $U/U_{mf} \geq 2.5$ a neutrally-buoyant behavior of the object was observed. The motion of the object in the freeboard and inside the dense bed was recorded with a high speed video-camera, using an acquisition frequency of 125 fps. The aim of this chapter was to study the object motion in the freeboard and its relation with the bubble in the ejection. Therefore, the measurement technique in this section was developed to be capable of distinguishing the object, the bubbles and the dense phase at the same time. During the tests, more than 1.5 million images were taken, corresponding to a running time of around 3.5 h. A

threshold was used to characterize the position of the object in all the images, obtaining the velocity of the object at each instant.

3.2.2 Data analysis

In the freeboard of the bed, the motion of a large object can be assumed to be defined by gravity since there are no other relevant interactions: the drag force of the air stream over the large object can be neglected, (0.056 m/s^2 for $U = 2.5U_{mf}$ in our case), the friction with the 2-D walls was proved to be hardly noticeable and interactions with the dense phase seldom occur. Therefore, when the object is in the freeboard, its motion follows a ballistic trajectory. Nevertheless, sometimes the object can collide with dense phase particles coming from previous bubble eruptions, and, in other occasions, it may hit with the 2-D bed width limits, modifying its trajectory.

Some conditions were established to extract the intervals of the ballistic motion from the discrete tracking measurements. First, the positions where the object reaches the highest height compared with its neighbors position were determined. These positions will from now on be referred as peaks of the object motion. Once the peaks were established, a test was performed for each one in order to find out whether the object was at the freeboard or not. For the peaks in the freeboard, the initial and final positions of the trajectory of the object in the freeboard were then established. This was performed using the following procedure. At first, a minimum path that consisted of the peak and the positions of the object in the four previous and four posterior images was established. Then, new points were added to the path at each side when the vertical velocity of the object was higher (in absolute value) than that of their immediate neighbor in the direction of the peak. When that is not the case, the next neighbor shows a lower velocity in absolute value, the ballistic path was considered complete and the initial and final positions of the object path were obtained. Then, a fitting of the vertical position of the path versus time was performed to check its ballistic behavior. Those paths that passed the test were considered as ballistic paths and the information of their initial velocity, displacement and time interval was determined. An example of an experimental trajectory of the object in the freeboard can be observed in Figure 3.1(a). The position of the object at each instant is plotted over the real image acquired by the camera corresponding to the last frame of the ballistic path sequence.

The initial and final point of the trajectory are marked with a blue cross. The vertical position of the object, y, in the trajectory showed in Figure 3.1(a)

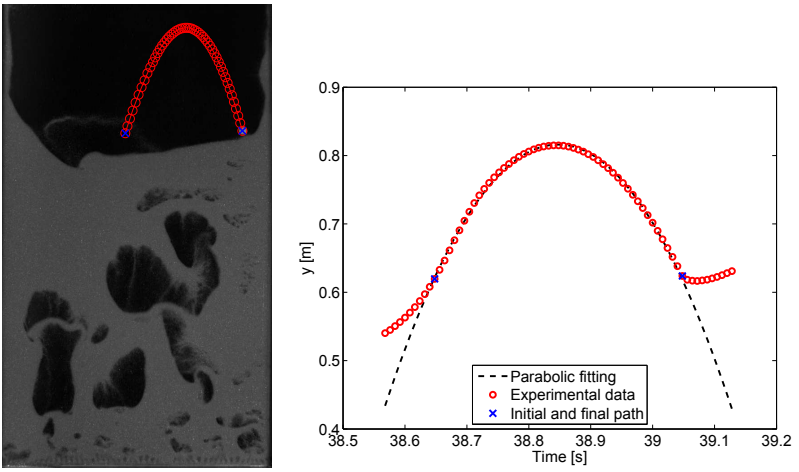

(a) (b)

Figure 3.1: Object trajectory plotted (a) over the real image and (b) with the parabolic fitting.

is plotted versus time in Figure 3.1(b) together with its parabolic fitting. The initial and final points of the trajectory are marked with blue crosses and some extra points before and after the initial and final points are also depicted in Figure 3.1(b). The parabolic fitting of the vertical positions is plotted with a black dash line, showing a very good match with the experimental trajectory and allowing to accept the assumption of a ballistic path. The method described to decide if a motion of the object in the freeboard is a ballistic motion was employed for all cases and the total of ballistic paths obtained was 750. Table 3.1 shows the number of the ballistic trajectories found for each case. Finally, the object lateral displacement and the time spent by the object in the ballistic trajectory can be calculated directly from the ballistic path trajectory.

Table 3.1: Ballistic paths obtained from the data analysis for each configuration.

	$h_{fb} = 0.3$ m				$h_{fb} = 0.5$ m				All
U/U_{mf}	1.8	2.3	2.8	3.4	1.6	2	2.5	3	-
Ballistic paths	54	124	69	66	64	166	92	115	750

3.3 Results

3.3.1 Experimental results for the object velocity

The ballistic motion of the object in the freeboard is described with the ejection velocity vector. In an opposite way, the ballistic paths obtained experimentally allows to determine the ejection velocity in each case. The ejection velocity vector can be expressed in terms of its modulus, U_{obj}, and angle, θ. This angle is here defined as the angle between the velocity vector and the vertical coordinate. Vertical symmetry was considered since the object was ejected to both sides of the bubble path with the same probability.

Both the modulus and the angle were obtained experimentally from the object ballistic trajectories in the freeboard. There is a general agreement that objects with proper circulation and dense phase are raised in fluidized beds by bubbles. Several works have studied the ejection velocity of the dense phase and its relation with the bubbles velocity, using experimental techniques (Fung & Hamdullahpur, 1993; Santana *et al.*, 2005; Almendros-Ibáñez *et al.*, 2006; Müller *et al.*, 2007) and numerical simulations (Hernández-Jiménez *et al.*, 2011). Nonetheless, there is no work available concerning the ejection velocity of a large object. For dense phase particles, the results for different authors differ. Fung & Hamdullahpur (1993) observed that the particles are ejected radially and with a velocity that correlates with the bubble velocity and the ejection angle. Correlations differ between different authors, but there is a certain agreement that particle velocities are larger than the bubble velocity and that there is a decrease of velocity for increasing ejection angle.

The ejection velocity for large objects may differ from that of the dense phase particles. The dense phase particles are subjected to the drag force of the gas flow, while the incidence of the gas drag force in large objects can be neglected as stated previously in section 3.2.2.

For comparison with the object ejection velocity, the mean bubble velocity can be calculated for the different cases employing the Davidson and Harrison correlation (Davidson & Harrison, 1963) and using the Shen correlation of the bubble diameter (Shen *et al.*, 2004). Both equations are implemented in Chapter 1 in equations (1.2) and (1.3) respectively.

The experimental results obtained for the object ejection velocity, modulus and angle are plotted in Figure 3.2. The results showed a similar behavior for every experimental configuration, varying U/U_{mf} and h_{fb}, and thus the results for all cases are plotted together.

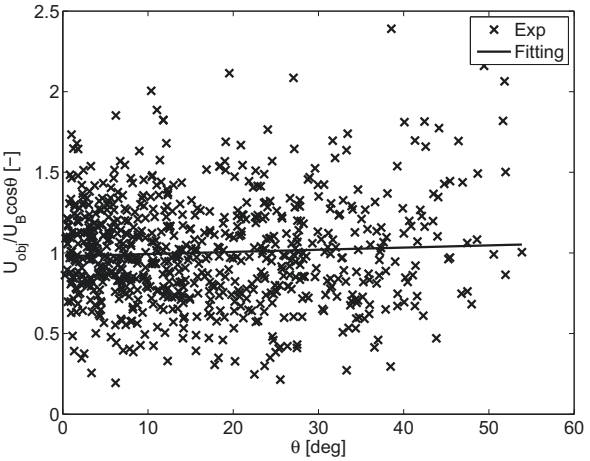

Figure 3.2: Relation between object and bubble velocity against the ejection angle.

The horizontal axis shows the ejection angle obtained, with values between 0 and 55°. Note that the ejection angle is defined as an absolute value. The vertical axis shows the ratio of the modulus of the object ejection velocity to the mean bubble velocity multiplied by the cosine of the ejection angle. The values of the object ejection velocity range between 0.2 and 2.4 times the mean bubble velocity multiplied by the cosine of the ejection angle.

The magnitude used in the vertical axis is extracted from the experimental results. The fitting of all experimental points is plotted as a black line, showing a constant value around unity for the whole range of ejection angles. Thus, the mean bubble velocity multiplied by the cosine of the ejection angle represents the mean value of the modulus of the object ejection velocity for the different experimental cases, showed in equation (3.1).

$$\overline{U_{obj}} = U_B \cos\theta \tag{3.1}$$

where $\overline{U_{obj}}$ is the mean value of the modulus of the object ejection velocity, U_B is the mean bubble velocity and θ is the object ejection angle.

The results suggest that objects move jointly with the bubbles prior to the ejection, and no other relevant forces are present at the instant of ejection. The dispersion of the data in Figure 3.2 may then correspond to differences between the mean bubble velocity and the instantaneous bubble velocity. The cosine dependence is in accordance with the decrease of the velocity for higher ejection angles showed in the dense phase ejection studies.

The dispersion of the data obtained for the object ejection velocity, in mod-

ulus and angle, should be treated separately. The distributions for both magnitudes are plotted in Figure 3.3. As stated previously, all the cases are plotted together. The results for the modulus of the object ejection velocity showed very similar distributions between different cases, while those for the ejection angle showed minor variations. Figure 3.3(a) shows the distribution of the ejection angle for all cases. The probability density function decreases exponentially with the ejection angle. Therefore, most of the ejections are grouped in the vicinity of the vertical direction, 75% of the ejection angles are below 30°. The experimental frequency histogram was integrated between 0 and 90° and normalized in order to obtain a probability density function, $p(\theta)$, presented in equation (3.2).

$$p(\theta) = 0.046 \exp(-0.045\theta) \tag{3.2}$$

The distribution of the experimental data for the modulus of the object ejection velocity, U_{obj}, is plotted in Figure 3.3(b) in dimensionless form with the bubble velocity times the cosine of the ejection angle. The figure shows a Gaussian distribution fitting, with a mean of 1.00 and a standard deviation of 0.32.

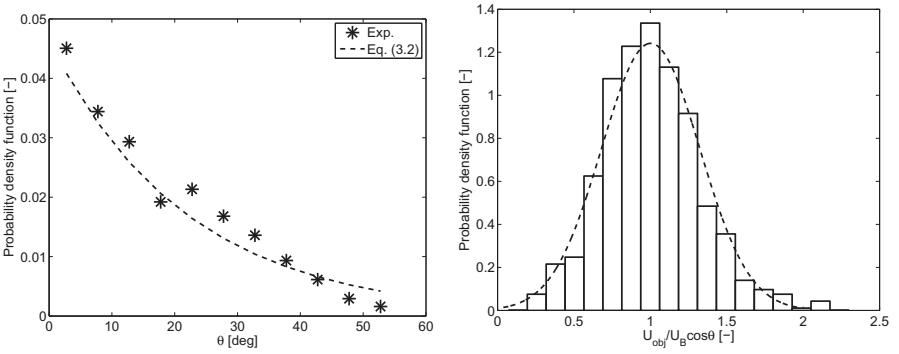

(a) (b)

Figure 3.3: Probability density function of (a) the ejection angle and (b) the ratio of object and bubble velocity.

3.3.2 Experimental results for the time of flight and lateral displacement

Once the ballistic path of the object in the freeboard was obtained, the time of flight of the object, t_f, and the lateral displacement, Δx, during its motion in the freeboard were measured. The experimental results are presented using box plots, giving the median value, the upper and lower quartile, 75% and 25% of the population, and a confidence interval. Outside of this confidence interval, the outliers are depicted, one by one.

The box plots of the time of flight for different dimensionless gas velocities, U/U_{mf}, are plotted in Figure 3.4(a) for a fixed bed height of 0.3 m and in Figure 3.4(b) for a fixed bed height of 0.5 m. The time of flight showed a Gaussian type distribution in all the cases, with medians ranging from 0.17 to 0.30 s. In both figures, the time of flight increases with the dimensionless gas velocity, and the relation seems to be quite linear for the median. These results are coherent with the previous reasoning: higher velocities and bed heights involve higher bubble velocities (see equations (1.2) and (1.3)), which produce higher object ejection velocities (equation (3.1)) and thus larger times of flight.

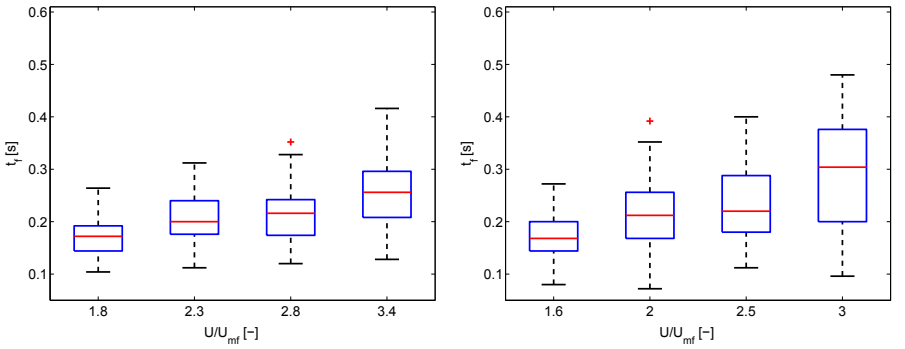

(a) (b)

Figure 3.4: Time of flight for fixed bed heights of (a) 0.3 m and (b) 0.5 m for different U/U_{mf}.

The number of ballistic paths needed for a proper statistical results was analyzed. The lower quartile, the upper quartile and the median of the time of flight were calculated considering a different number of ballistic paths. The dispersion of the values of time of flight for the case of $U/U_{mf} = 3$ and bed height of 0.5 m is plotted in Figure 3.5, as a function of the number of ballistic

paths considered. This case was selected to determine the number of ballistic paths needed for proper statistics since the dispersion of the time of flight is the highest, as can be seen in Figure 3.4. The values of the statistical parameters of the time of flight showed a large dispersion when considering less than 50 ballistic paths, being the parameters uniform up to this point as can be observed in Figure 3.5. Therefore, according to these data the number of ballistic paths obtained from the experiments and presented in Table 3.1 are sufficient to ensure proper statistical results.

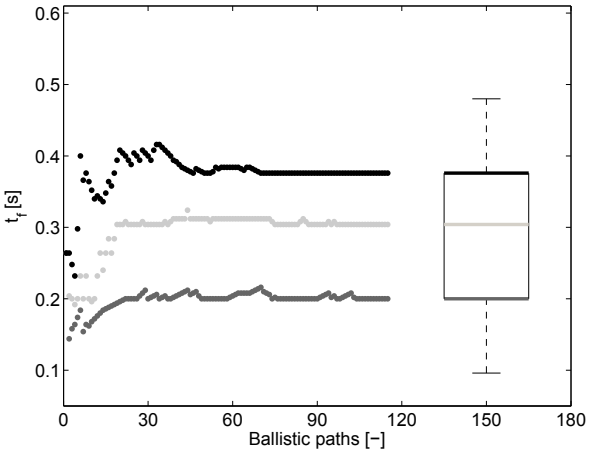

Figure 3.5: Variation of the lower quartile, median and upper quartile of the time of flight as a function of the number of ballistic paths.

The lateral displacement of the object in the freeboard was defined as the horizontal distance between the final and initial positions of the ballistic trajectory. Experimentally, the lateral displacement could not be obtained directly in a number of ejections, since hits with the width limits occur during the ballistic trajectory. In such cases, the lateral displacement was calculated considering the object trajectory until it hits with the width limits and extrapolating the results employing the total time of flight.

The results of the lateral displacement are plotted for the 0.3 and 0.5 m fixed bed heights in Figure 3.6(a) and Figure 3.6(b) respectively. In both cases, the lateral displacement increases with the gas velocity. The median values obtained experimentally varying between 0.03 m and 0.1 m.

The vertical difference between the initial and final position of the object ballistic trajectory in the freeboard can also be calculated directly from the experimental data. The results are plotted in Figure 3.7.

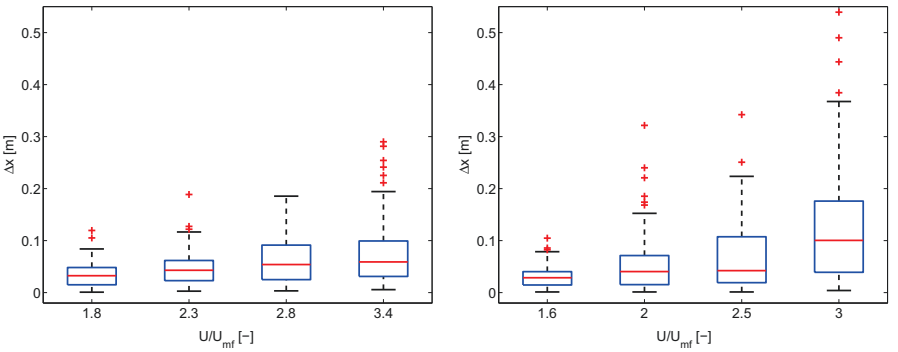

(a) (b)

Figure 3.6: Lateral displacement for fixed bed heights of (a) 0.3 m and (b) 0.5 m for different U/U_{mf}.

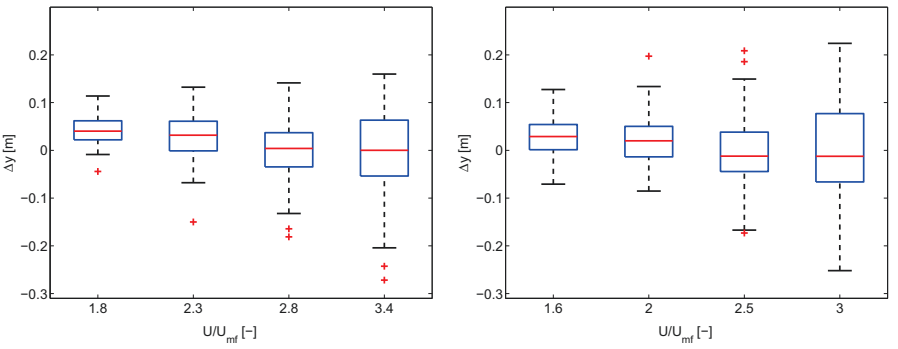

(a) (b)

Figure 3.7: Vertical difference between initial and final position for fixed bed heights of (a) 0.3 m and (b) 0.5 m for different U/U_{mf}.

For low dimensionless gas velocities, $U/U_{mf} < 2.5$, a positive vertical difference between the initial and final position can be observed, while for higher gas velocities the tendency is canceled. The results may be explained as representing the two behaviors of the object for the different U/U_{mf}. For low dimensionless velocities, $U/U_{mf} < 2.5$, the flotsam object is located most of the time at the top of the bed and moves jointly with the bubble when the bubble starts the eruption. Therefore the object needs to be accelerated prior to its ejection and is generally ejected at a higher height than that of the surface of the bed, where the object is more prone to finish the ballistic path. On

the other hand, with a proper circulation of the object, $U/U_{mf} \geq 2.5$, it raises jointly with the bubble. Thus, the ejection of the object starts at the time of the bubble eruption and the initial and final position of the parabolic path are similar.

Nevertheless, the vertical differences are slight. The median values range from -0.01 m and 0.04 m as can be observed in Figure 3.7(a) and Figure 3.7(b). Therefore, in a first approximation the vertical difference can be considered negligible.

3.3.3 Model based on Monte Carlo simulations

A model is proposed to estimate the time of flight and the lateral displacement of a large object moving in the freeboard of the fluidized bed, based on its ejection velocity, modulus and angle. As stated in the experimental results for the object velocity, section 3.3.2, these parameters follow different type of statistical distributions. Thus, using mean values, these parameters are not represented with high accuracy, and a Monte Carlo simulation is needed for more accurate results. The Monte Carlo simulations were performed using a MatLab® algorithm. The inputs were obtained from the experimental results: i) the Gaussian distribution for the relation between the object ejection velocity and the bubble velocity times the cosine of the ejection angle, and ii) the exponential probability function of the ejection angle expressed by equation (3.2). The main hypothesis of the model based on Monte Carlo simulations is that these two distributions are independent, an assumption based on the results showed in Figure 3.2. The time of flight calculated in the Monte Carlo model, $t_{f,MC}$, is based on the ballistic equation (3.3).

$$t_{f,MC} = \frac{V_{oy,MC} + \sqrt{V_{oy,MC}^2 + 2 \cdot g \cdot \Delta y}}{g} \tag{3.3}$$

where $V_{oy,MC}$ is the vertical velocity of the object ejection obtained by the simulation, g is the gravity and Δy is the vertical difference between the initial and final position of the ballistic path.

The vertical difference was assumed to be negligible in order to simplify the model. The vertical component of the object ejection velocity can be written in terms of the modulus of the ejection velocity and the ejection angle. Then, the time of flight can be calculated as equation (3.4).

$$t_{f,MC} = \frac{2 \cdot U_{obj,MC} \cos\theta_{MC}}{g} \tag{3.4}$$

where $U_{obj,MC}$ is the modulus of the object ejection velocity obtained by the Monte Carlo simulations, and θ_{MC} is the ejection angle obtained by Monte Carlo simulations.

A total number of 10^5 Monte Carlo simulations were run for each case, considering the probability density functions of the ejection angle and the Gaussian distribution of the relation between the modulus of the object ejection velocity and the bubble velocity times the cosine of the ejection angle, obtained experimentally as inputs. Then, the outputs of the Monte Carlo simulations were the distributions of the time of flight and the lateral displacements. In Figure 3.8, the box plots of the time of flight calculated by the Monte Carlo simulations are plotted for the different cases. The time of flight increases with the dimensionless gas velocity for both heights, showing a linear tendency. In the Monte Carlo simulation results, there are values of the time of flight equal to zero in contrast to the experimental results, where a minimum time spent by the object in the freeboard is necessary during the data analysis procedure. Apart from that, the results obtained in the simulations are in a good agreement with the experimental data shown in Figure 3.4. Obviously, the number of outliers obtained for 10^5 simulations is far larger than the number of those obtained in the experiments, so they are not depicted for the Monte Carlo simulation results.

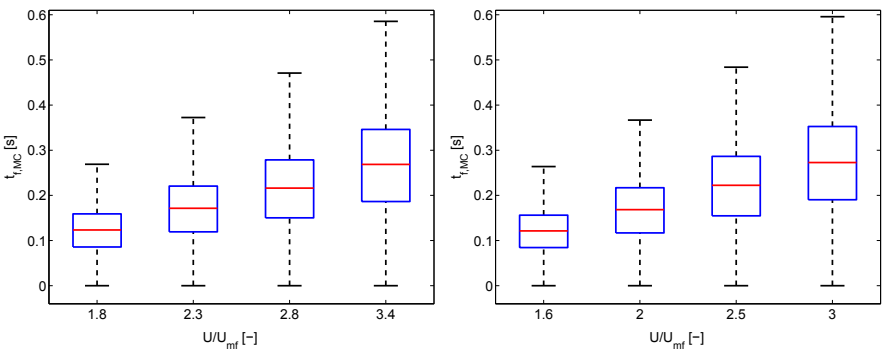

(a) (b)

Figure 3.8: Time of flight for Monte Carlo simulations for fixed bed heights of (a) 0.3 m and (b) 0.5 m for different U/U_{mf}.

The lateral displacement, Δx_{MC}, can be calculated with equation (3.5) using the output parameter of the Monte Carlo simulations, i.e. the time of

flight, $t_{f,MC}$.

$$\Delta x_{MC} = U_{obj,MC} \sin\theta_{MC} \cdot t_{f,MC} \tag{3.5}$$

The results of the lateral displacement are plotted in Figure 3.9. Similar to the case of the time of flight, the lateral displacement increases with a linear tendency with the gas velocity and the influence of the fixed bed height can also be considered negligible. The results obtained by the simulations show a good agreement with the experimental data shown in Figure 3.6.

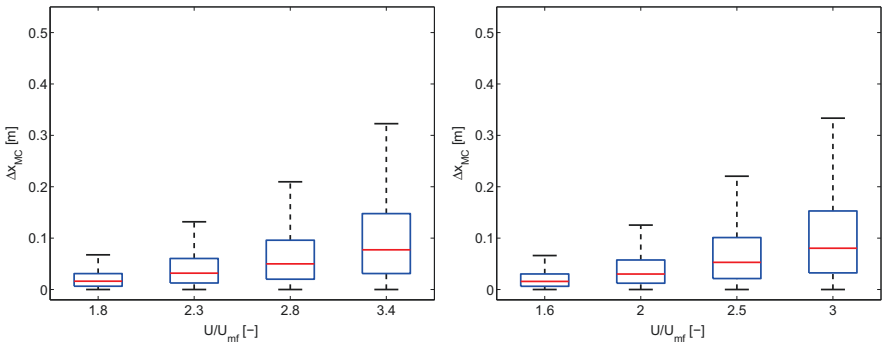

Figure 3.9: Lateral displacement for Monte Carlo simulations for fixed bed heights of (a) 0.3 m and (b) 0.5 m for different U/U_{mf}.

The mean bubble velocity was the only difference between cases for the inputs in the Monte Carlo simulations and, as stated in equations (1.2) and (1.3), it is a function of the operational conditions. Therefore, a dimensionless form of the time of flight and lateral displacement was proposed to obtain a collapse of Monte Carlo results for all the cases. The dimensionless form for the time of flight, τ, obtained from equation (3.4) is expressed in equation (3.6), as a function of the mean bubble velocity and the average of the square of the cosine for all the ejection angle distribution, calculated by the simulations. The value obtained for such average is 0.823 and is in good agreement with that obtained experimentally.

$$\tau = \frac{t_f}{2 \cdot U_B \cdot 0.823/g} \tag{3.6}$$

In the case of the lateral displacement, the dimensionless form used, ψ, can be obtained from equation (3.5). The object velocity was expressed in

equation (3.7) as a function of the mean bubble velocity and the average of the cubic of the cosine times the sine for all ejection angles obtained from the simulations. The value obtained for that average is 0.182.

$$\psi = \frac{\Delta x}{2 \cdot U_B^2 \cdot 0.182/g} \tag{3.7}$$

The probability density function of the dimensionless form of the time of flight (equation (3.6)), calculated by the Monte Carlo simulations, is plotted in Figure 3.10(a). The data obtained shows a Gaussian distribution with a mean value of 1.00 and standard deviation of 0.44. The results converge for all cases to the same curve. In the case of the lateral displacement, the probability density function of the results of the dimensionless form using equation (3.7) is plotted in Figure 3.10(b). The results correspond with an exponential distribution with a rate parameter of 1.10. The figures show a good agreement between the proposed distributions and the Monte Carlo results. Again, the results for all cases collapsed to the same curve.

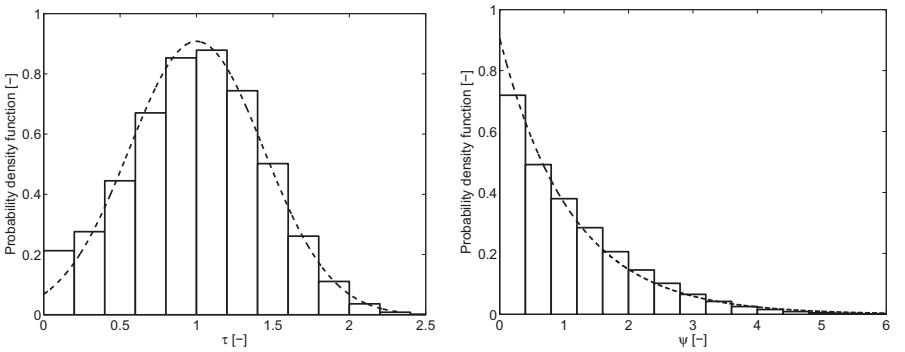

(a) (b)

Figure 3.10: Probability density functions of (a) dimensionless time of flight and (b) dimensionless lateral displacement.

3.4 Discussion

The Monte Carlo simulation and the experimental results were compared in order to validate the proposed model employing the dimensionless form for the time of flight and the lateral displacement respectively. The comparison between the experimental results and the Monte Carlo simulations of the dimensionless form of the time of flight is plotted in Figure 3.11 for different

dimensionless gas velocities and fixed bed heights. The simulation results are plotted only once since the distributions are identical for all cases, as stated in the previous section. The simulation and the experimental results for the dimensionless form of the time of flight shows a general good agreement. Furthermore, $\tau = 1$ represents quite well the median values of the results for the proper circulation behavior cases. The experimental results show a small discrepancy for lower gas velocities, where the median values are slightly larger than unity. This effect may be attributed to the vertical difference between the initial and final position in the ballistic motion, linked to the flotsam behavior of the object at these velocities.

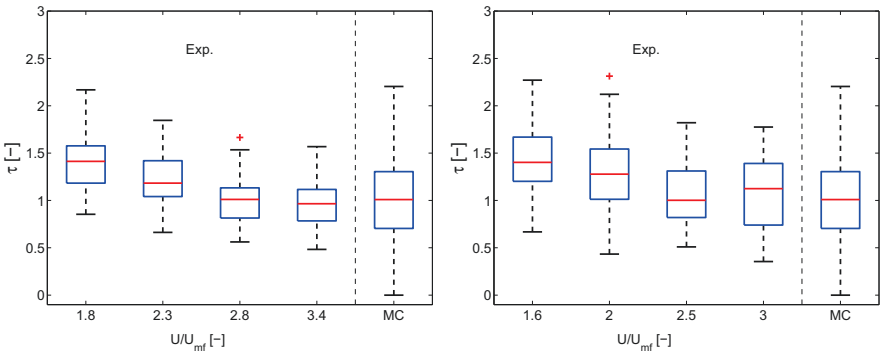

(a) (b)

Figure 3.11: Dimensionless time of flight comparison between experimental and Monte Carlo results for fixed bed heights of (a) 0.3 m and (b) 0.5 m for different U/U_{mf}.

Figure 3.12 shows the dimensionless results of the lateral displacement, obtained experimentally and simulated using the Monte Carlo model for different dimensionless gas velocities and fixed bed heights. Again, the simulation results are plotted only once since the distributions are identical. The dimensionless forms show a general good agreement between the simulation and the experimental results for the proper circulation behavior. Furthermore, $\psi = 1$ represents quite well the median value of the results. The tendency to larger dimensionless displacements for lower gas velocities is similar to that observed for the time of flight, and can be attributed to the flotsam behavior of the object at these velocities.

The values of the dimensionless form of the time of flight and the lateral displacement obtained from the Monte Carlo simulations are in good agreement

with the experimental results for neutrally-buoyant objects ($U/U_{mf} \geq 2.5$). Therefore, the time of flight and the lateral displacement of a large object motion in the freeboard can be calculated only as a function of the operational conditions of the fluidized bed with high accuracy.

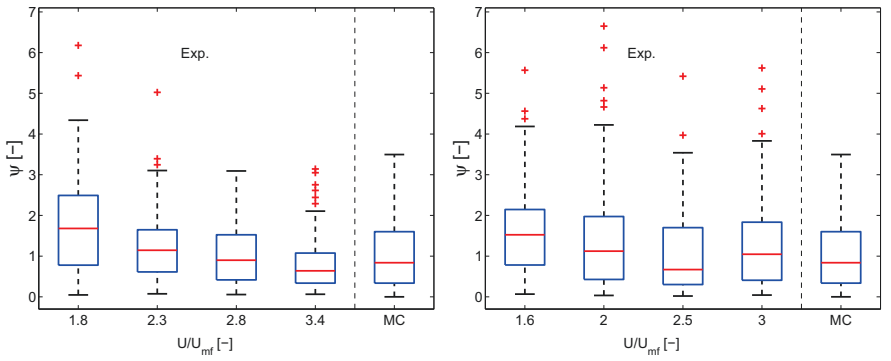

Figure 3.12: Dimensionless lateral displacement comparison between experimental and Monte Carlo results for fixed bed heights of (a) 0.3 m and (b) 0.5 m for different U/U_{mf}.

For a better estimation of the flotsam behavior cases, new Monte Carlo simulations were run considering the vertical differences between initial and final position of the ballistic path. These vertical differences were set using the median values obtained experimentally and showed in Figure 3.7. This vertical difference was positive for the cases of flotsam behavior, therefore a larger time of flight and lateral displacement were obtained, according to equations (3.3) and (3.5). In Figure 3.13 and Figure 3.14 the comparison between the experimental results and the Monte Carlo simulations for τ and ψ are plotted for the flotsam cases.

For both parameters the comparison between the experimental results and the Monte Carlo simulations show a better concordance when considering the vertical difference between the initial and final position of the parabolic motion.

The results presented from Figure 3.11 to Figure 3.14 showed that the experimental data for the time of flight and the lateral displacement could be simulated with different levels of accuracy and simplicity. A first approximation can be obtained using $\tau = 1$ and $\psi = 1$. This gives good approximations for the representative values of the time of flight and lateral displacement but no information about the probability density function. Another, more accurate,

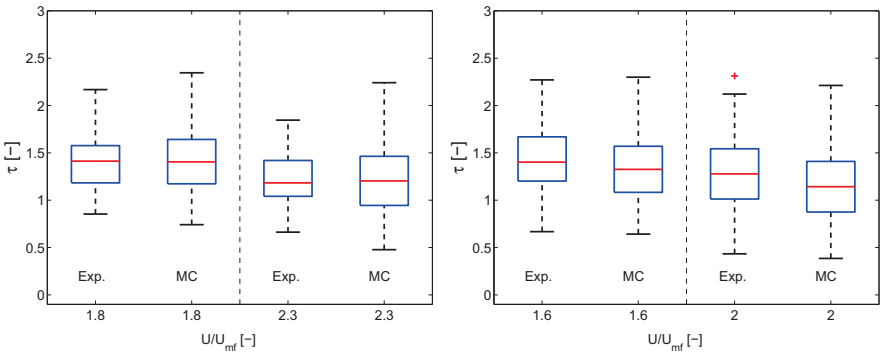

(a) (b)

Figure 3.13: Comparison of the dimensionless time of flight between experimental and Monte Carlo results for fixed bed heights of (a) 0.3 m and (b) 0.5 m for the flotsam cases.

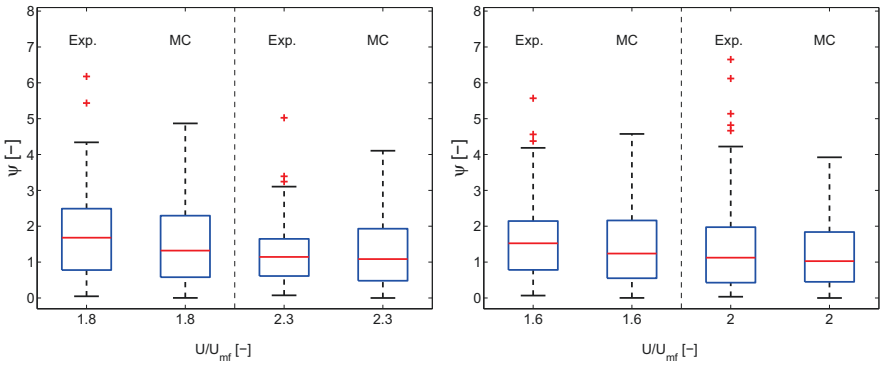

(a) (b)

Figure 3.14: Comparison of the dimensionless lateral displacement between experimental and Monte Carlo results for fixed bed heights of (a) 0.3 m and (b) 0.5 m for the flotsam cases.

approximation is to employ the Gaussian distribution for the time of flight, given by a mean value and a standard deviation of 1.00 and 0.44 respectively. In the case of the lateral displacement, the probability density function is defined with a rate parameter of the exponential distribution, equal to 1.10. A third approximation is to perform the Monte Carlo simulations following the simple model established in section 3.3.3. This will give reliable probability density functions for the two parameters. Finally, if a high accuracy is needed

when describing the ejection of flotsam objects, the vertical differences between the initial and final position of the ballistic path should also be considered in the Monte Carlo simulations, whereas these differences are negligible for objects with a proper circulation throughout the bed.

3.5 Conclusions

This chapter shows experimental and simulation results for the motion of a large and non-reacting object in the freeboard of a 2-D bubbling fluidized bed. A tracking technique was developed in order to study its motion. Several experimental conditions were employed, varying the gas velocity and the fixed bed height. Two different behaviors of the object were studied, employing a flotsam object. The motion was characterized and compared to a ballistic behavior described by the modulus and angle of the ejection velocity. The first one was related with the mean bubble velocity times the cosine of the ejection angle, showing a Gaussian distribution with a mean value around unity. On the other hand, the ejection angles are in the range of 0 and 55°. The experimental data showed an exponential decrease of the probability of the ejection angle when the angle increases. The time of flight and the lateral displacement of a large object while it is in the freeboard were obtained directly from the experimental data. For both parameters, a linear increment when increasing the gas velocity was observed. The median of the time of flight ranges from 0.17 to 0.30 s, while the median of the lateral displacement obtained varied from 0.03 to 0.1 m. The vertical difference between the initial and final position of the ballistic path was also calculated showing differences between lower and higher dimensionless gas velocity, according to the different behavior of a flotsam object when increasing the gas velocity.

A Monte Carlo model was developed based on the kinematic equations of the ballistic motion and the probability distribution for the modulus and angle of the object ejection velocity obtained from the experimental results. The Monte Carlo simulations were run for 10^5 objects for each experimental configuration, obtaining the time of flight and lateral displacement for each case. A dimensionless form based on the mean bubble velocity, operational conditions of the bed, and average values of the ejection angle distribution was used to compare the time of flight and lateral displacement between the experimental results and the Monte Carlo simulations. The dimensionless forms showed small discrepancies for lower gas velocities, associated with the flotsam object

behavior.

Finally, three different approximations are proposed to calculate the time of flight and lateral displacement. The approximations described the object motion in the freeboard with different degrees of accuracy.

Notation

g	Gravity [m·s^{-2}]
h_{fb}	Fixed bed height [m]
$p\,(\theta)$	Probability density function for the ejection angle [−]
t_f	Experimental time of flight [s]
$t_{f,MC}$	Simulation time of flight [s]
U	Superficial gas velocity [m·s^{-1}]
U_B	Bubble velocity [m·s^{-1}]
U_{mf}	Minimum fluidization velocity [m·s^{-1}]
U_{obj}	Modulus of the object ejection velocity [m·s^{-1}]
$\overline{U_{obj}}$	Mean value of the modulus of the object ejection velocity [m·s^{-1}]
$U_{obj,MC}$	Modulus of the object ejection velocity obtained by simulation [m·s^{-1}]
$V_{oy,MC}$	Vertical component of the object ejection velocity obtained by simulation [m·s^{-1}]
Δx	Experimental lateral displacement in the x-direction [m]
Δx_{MC}	Simulation lateral displacement in the x-direction [m]
y	Vertical position of the object [m]
Δy	Vertical difference between the initial and final position of the object in the ballistic path [m]
τ	Dimensionless form of time of flight [−]
θ	Ejection angle [deg]
θ_{MC}	Ejection angle obtained by simulation [deg]
ψ	Dimensionless form of lateral displacement [−]

References

Almendros-Ibáñez, J.A., Sobrino, C., de Vega, M. & Santana, D. 2006 A new model for ejected particle velocity from erupting bubbles in 2-D

fluidized beds. *Chemical Engineering Science* 61 (18), 5981 – 5990.

Davidson, J.F. & Harrison, D. 1963 *Fluidised particles*, 1st edn. Cambridge: Cambridge University Press.

Fung, A.S. & Hamdullahpur, F. 1993 A gas and particle flow model in the freeboard of a fluidized bed based on bubble coalescence. *Powder Technology* 74 (2), 121 – 133.

Hernández-Jiménez, F., Third, J.R., Acosta-Iborra, A. & Müller, C.R. 2011 Comparison of bubble eruption models with two-fluid simulations in a 2d gas-fluidized bed. *Chemical Engineering Journal* 171 (1), 328 – 339.

Müller, C.R., Davidson, J.F., Dennis, J.S. & Hayhurst, A.N. 2007 A study of the motion and eruption of a bubble at the surface of a two-dimensional fluidized bed using particle image velocimetry (PIV). *Industrial & Engineering Chemistry Research* 46 (5), 1642 – 1652.

Santana, D., Nauri, S., Acosta, A., García, N. & Macías-Machín, A. 2005 Initial particle velocity spatial distribution from 2-D erupting bubbles in fluidized beds. *Powder Technology* 150 (1), 1 – 8.

Shen, L., Johnsson, F. & Leckner, B. 2004 Digital image analysis of hydrodynamics two-dimensional bubbling fluidized beds. *Chemical Engineering Science* 59 (13), 2607 – 2617.

CHAPTER
FOUR

Simulation of object motion inside the dense bed using a Monte Carlo method

Contents

4.1 Introduction

The motion of a large neutrally-buoyant and non-reacting object immersed in a 2-D bubbling fluidized bed was modeled and simulated using a Monte Carlo method. The characteristics of the object vertical trajectory inside the dense bed were established for a range of dimensionless gas velocities using a simple 1-D model. The main parameters that define the object motion were obtained, either from experiments of previous works or from new experiments for this purpose. Then, the 1-D trajectory was determined using the Monte Carlo method, and the main parameters of the object motion obtained from the simulations were compared with experimental evidence. On a second step,

the time scale of the motion is introduced in the simulated data by means of the object sinking and rising velocities, obtained as a function of well-known 2-D correlations for the bubble and dense phase velocities. The circulation time of an object, from the instant when it leaves the freeboard and sinks in the dense bed till the moment it reappears back on the surface, was then obtained and compared with experimental data. Finally, the Monte Carlo model was extrapolated to a 3-D fluidized bed and the validity of the extrapolation was discussed based on experimental measurements of the circulation time in a lab-scale 3-D fluidized bed.

4.2 Experimental setup

Some experimental or theoretical results are needed to provide inlet data for the Monte Carlo simulations and to validate the simulation results. This is achieved by referring to experiments and to well-known correlations in the literature presented in Chapter 1. Nevertheless, some experiments have been carried out to cope with specific aspects.

A detailed description of the measurement techniques can be found in sections 2.3.1 and 2.3.3. In this section, a brief description of the experimental procedure is presented.

The experimental facilities employed in this chapter consisted of two bubbling fluidized beds: a 2-D bed with a thickness of 0.010 m, and a lab-scale 3-D bed, which characteristics were described in sections 2.1 and 2.2 respectively. The height of the fixed bed was 0.5 m for the 2-D bed and 0.192 m for the 3-D lab-scale bed, corresponding to an aspect rate of one in both cases. The bed material for both experimental facilities was spherical ballotini particles, with a diameter range of 600-800 μm and the bed density was 1560 kg/m^3. The object used during the tests was that with cylindrical shape and covered with strontium aluminate, being its density equal to 1508 kg/m^3. Thus, the buoyancy effects could be considered negligible, and the object is further referred to as neutrally-buoyant. The dimensionless gas velocity employed during the 2-D experiments was set to 2, 2.5 and 3, while during the tests in the 3-D lab-scale was 2 and 2.5 since the highly vigorous fluidization for $U/U_{mf} = 3$ prevented the accurate detection of the object in the splashing zone. Table 4.1 provides general information about the experimental setup used during the test presented in this chapter.

Table 4.1: General information about the experimental setup.

2-D bed facility	
Bed height [m]	2
Bed width [m]	0.5
Bed thickness [m]	0.010
Fixed bed height [m]	0.5
Minimum fluidization velocity (U_{mf}) [m/s]	0.32
Dimensionless gas velocity (U/U_{mf}) [-]	2; 2.5; 3
3-D bed facility	
Bed height [m]	1
Bed diameter [m]	0.192
Fixed bed height [m]	0.192
Minimum fluidization velocity (U_{mf}) [m/s]	0.25
Dimensionless gas velocity (U/U_{mf}) [-]	2; 2.5
Bed material (in both beds): ballotini particles	
Particle diameter [μm]	600-800
Skeletal density [kg/m^3]	2500
Bulk density [kg/m^3]	1560
Object	
Length [m]	0.019
Diameter [m]	0.0064
Density [kg/m^3]	1508

4.3 Monte Carlo simulation

4.3.1 Numerical method

A 1-D model was developed, based on two external parameters obtained experimentally: i) the probability of an object in a rising path to arrive at the surface of the bed directly by the action of a single bubble, p, and ii) the probability of the object to start a rising path when arriving to a certain depth, $q\,(d_j)$. The bed height was divided in 10 slices of 0.05 m, between a position defined by the

fixed bed height (depth=0) and the bottom of the bed (depth=0.5 m).

A Monte Carlo method was used to simulate the vertical trajectory of the object, employing as input data the statistical parameters. The simulation was run for 10^7 objects. The procedure is schematized in Figure 4.1. The first object ($o = 1$) starts to sink and arrives to the first slice ($j = 1$), where two possibilities appear: to continue sinking or to start a rising path. Thus, a random number between 0 and 1 is generated, N_q. Then, the object continues sinking to the next slice ($j = j + 1$) if the number is greater than the probability of starting a rising path in this slice $q(d_j)$. In that case, another random number, N_q, is generated and the process is repeated. But if the random number is less than or equal to $q(d_j)$, the object starts a rising path. In order to state whether the object reaches the bed surface during that rising path or not, a new random number, N_p, between 0 and 1 is generated. Its value is compared with the average probability of an object to get directly to the bed surface, p, in that rising path. A value of N_p less than or equal to p means that the object reaches directly the bed surface, so the cycle is completed and another object ($o = o+1$) is simulated. Nevertheless, if N_p is greater than p, the object is considered to detach from the bubble before reaching the bed surface, in a position i between slice j and 1, and a new sinking process begins.

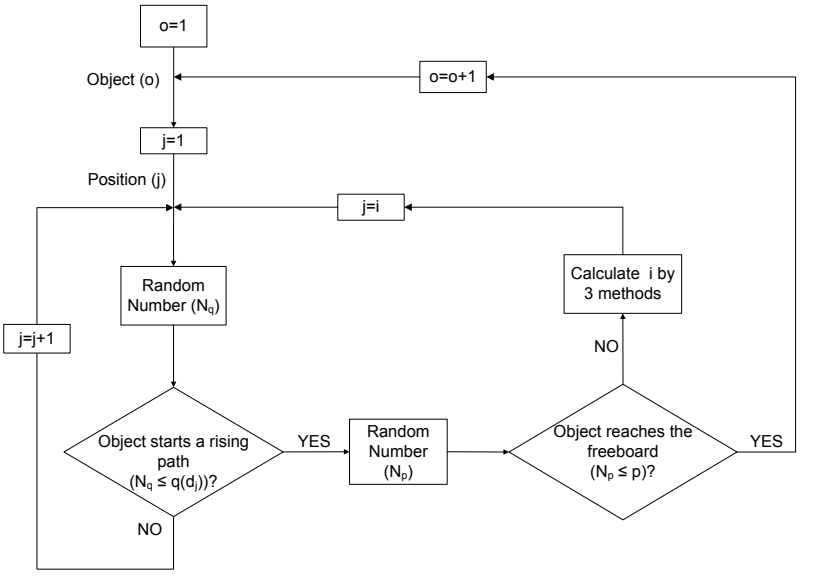

Figure 4.1: Scheme of the Monte Carlo model.

4.3.2 Inlet data

The Monte Carlo simulation was based on some inlet data, which were obtained from experimental results reported in the literature, new experiments or well established models. The inlet data required for the model are:

- the probability of an object to reach the bed surface by the action of a single bubble when starting a rising path, p,
- the probability of the object to start a rising path when arriving to a certain depth $q\,(d_j)$,
- a parameter that establishes at which position, i, the object is detached in its rising path when it is not able to reach directly the bed surface, and
- the sinking and rising velocities of the object.

The first three parameters allow to run the Monte Carlo simulation of the 1-D trajectories. The object velocities are used to determine the time scale of each rising and sinking trajectory. The values of p and $q(d_j)$ can be obtained experimentally. The detaching position of the object in the rising path, i, was modeled using different approaches and the results were compared in order to state the influence of the different assumptions. The object rising and sinking velocities are referred to the mean bubble and dense phase velocities obtained from well-known correlations.

The probability of an object to reach directly the surface, p, was experimentally obtained for a 2-D bed by Soria-Verdugo *et al.* (2011), as previously described in detail in section 1.2. The probability density function of the number of jumps, N_{jumps}, was found to follow a geometric law in the form of equation (1.4).

When an object starts a rising path with a bubble, there is a probability to reach the bed surface directly in that path and a complementary probability to detach from that bubble before arriving to the surface, starting a new sinking path. The form of the probability density function in equation (1.4) permits to consider the value of such a probability as that of parameter p, being $(1-p)$ the detaching probability. The parameter p obtained from this geometrical fitting is a mean parameter for the whole height of the bed, disregarding the depth at which each jump began. Therefore, the value of p will be considered constant and equal to 0.45.

The probability of starting a rising path when arriving to a certain depth, $q(d_j)$, was experimentally obtained for the 2-D bed conditions stated in section

4.2, dividing the bed height in ten slices of 0.05 m and determining the probability of the object to start a rising path at these discrete depths, d_j. The probability of an object to start a rising path in each slice is plotted in Figure 4.2. The depth of the bed was defined with origin at the fixed bed height, thus a height of 0.5 m corresponded to a depth of 0 m. The discrete depth, d_j, is presented in dimensionless form using the fixed bed height, h_{fb}, being 0 the surface of the bed and 1 the bottom. It was observed that the average probability of starting a rising path was a constant approximately equal to 20% for most of the bed and then sharply increased up to 100% at the bottom of the bed, where an object can only start a rising path. The probability of the object to start a rising path at each discrete depth, $q(d_j)$, was normalized to obtain the probability of starting a rising path for a continuous depth, $q\,(d)$. This normalized probability of starting a rising path for any depth is expressed in equation 4.1.

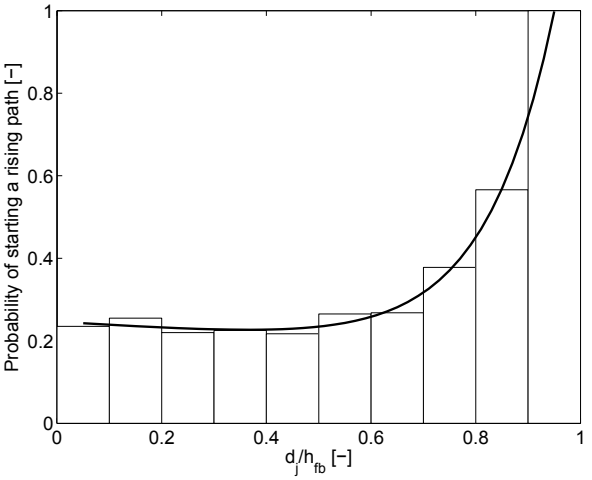

Figure 4.2: Probability of an object to start a rising path for each depth.

$$q(d) = 0.671 \exp(-0.343 d/h_{fb}) + 0.002 \exp(7.57 d/h_{fb}) \tag{4.1}$$

where d is the continuous depth and h_{fb} the fixed bed height.

Finally, the parameter i that establishes the position where the object is detached in its rising path should be obtained. This parameter is unknown and the present experiments cannot supply sufficient statistics for a proper characterization. Therefore, several limit cases have been defined. These cases are not used as facts but as limits. An object that rises but do not get to the

surface of the bed directly might detach from the bubble that is raising it i) with equal probability anywhere in the rising path, ii) with more probability at the beginning of the rising path. The actual process should be somewhere between these two limits.

Therefore, in a first case that will be called random loss case, the probability of the object to detach from the bubble is considered constant for each i position between the position where the object starts to rise, j, and the first position underneath the freeboard ($j = 1$). The second assumption will be divided in two cases to account for some differences when the rising path begins in the first upper slice. Therefore, in a second case, called maximum loss 1, the object was supposed to detach from the bubble immediately (at position $j-1$), except for the particular case of $j = 1$ where the object should remain in the same slice ($j = 1$). Here, a small variation can be considered, giving a third case called maximum loss 2. In this case, the object was supposed to detach from the bubble at position $j-1$ for any initial rising position, even for $j = 1$. Thus, in these case, an object that starts to rise in $j = 1$ will arrive to the bed surface with a probability of 100%. This contradicts the statement made for p, but was found to be a useful assumption. Equations (4.2) to (4.4) show the three cases:

$$\text{Random loss}: \quad i = \text{random}\,[1, j] \tag{4.2}$$

$$\text{Maximum loss 1}: \quad i = \begin{cases} j-1 & j \neq 1 \\ j & j = 1 \end{cases} \tag{4.3}$$

$$\text{Maximum loss 2}: \quad i = j - 1; \forall j \tag{4.4}$$

where i is the position where the object is detached in its rising path and j denotes the slice number.

The object trajectories can be obtained using a Monte Carlo method once the values of p, $q(d_j)$ and i are known. But a time scale was not yet available for the proper evaluation of the simulation. This time scale can be introduced by means of a characteristic sinking and rising object velocity for each bed position. The sinking velocity for a neutrally-buoyant object can be considered equal to the dense phase downwards velocity, which can be obtained using the Kunii & Levenspiel (1991) correlation. The bubble velocity was estimated using the correlation of Davidson & Harrison (1963) and the Shen *et al.* (2004) correlation for the bubble diameter. These correlations are formulated in Chapter 1 in equations (1.1), (1.2) and (1.3) respectively. For these PhD thesis it was assumed that the rising velocity of a neutrally-buoyant object is 20% the mean bubble velocity, as obtained by the previous works reviewed in section 1.2.

4.3.3 Validation

The numerical method was run for 10^7 objects and some comparisons were made in order to validate the procedure. First, it should be established that the number of objects was sufficient for proper statistics. Figure 4.3 shows the median of the circulation time of an object, defined as the time between the moment when the object leaves the freeboard and that when it reaches back to it, obtained for different runs of the numerical computation as a function of the number of objects used in the calculation. The results showed that a convergence can be ascertained for a number of objects larger than 10^6. Therefore, the number of objects employed in this study, 10^7 objects, can be said to provide proper statistical results.

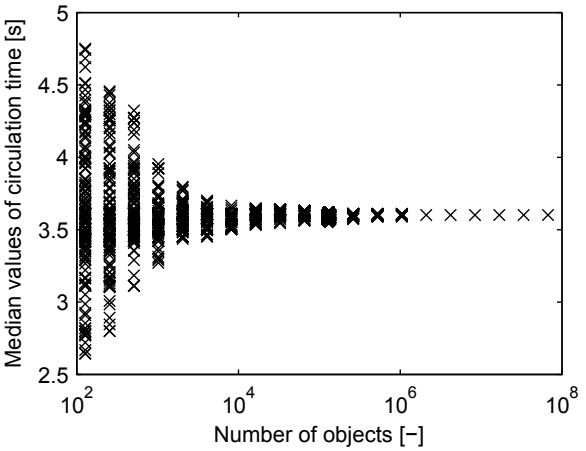

Figure 4.3: Median of the circulation time as a function of the number of objects used for the simulation.

The probabilities p and $q(d_j)$ were also obtained from the Monte Carlo simulation data for validation purposes and to determine the effect of the deviation introduced by the assumption in the maximum loss 2 case on the value of p. The results for $q(d_j)$ fit exactly the experimental data shown in Figure 4.2. The results for the random loss case and the maximum loss 1 case represent exactly the geometric law with $p = 0.45$, whereas the deviation that the maximum loss 2 case produced can be observed in Figure 4.4. The experimental data for a neutrally-buoyant object at $U/U_{mf} = 2.5$ presented in Figure 1.2 in Chapter 1, the geometric law represented in equation (1.4) with $p = 0.45$, and the results of the simulation for the maximum loss 2 case are plotted together

in Figure 4.4. The results showed that a minor effect exists as the $j = 1$ condition increases the probability for $N_{jumps} = 1$, but it still fits properly with the experimental results, and notably better for the probability of $N_{jumps} = 1$.

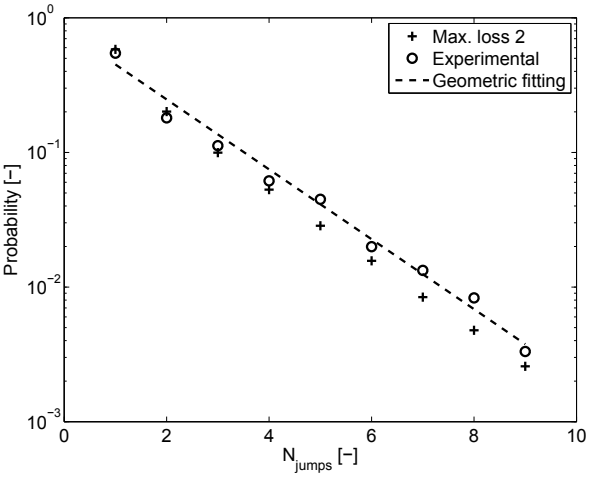

Figure 4.4: Probability of a certain number of jumps occurring in a cycle.

4.4 Results and discussion

The Monte Carlo simulation provides a complete temporal description of the object trajectories within the bed. In this section, simulation results will be compared with independent experimental results in order to establish the model accuracy representing the object motion inside the dense bed. First, some parameters of the object motion will be compared with experiments already presented in section 1.2, and then the circulation time distribution will be presented and compared with experimental results in a 2-D bed and with new experimental data obtained in the lab-scale 3-D bed presented in section 2.2.

4.4.1 Object motion inside the dense bed

The probability of finding an object at a certain height and the probability of an object to attain a certain maximum depth in a cycle, were experimentally obtained as characteristic parameters of the object motion by Soria-Verdugo *et al.* (2011) and reviewed in section 1.2. The former parameter identifies the capability of the fluidized bed to circulate the object throughout the whole

bed and the latter characterized the object cycles. In this section, both probabilities were calculated from the Monte Carlo results and compared with the experimental data.

The procedure for calculating the probability of finding an object at a certain height from the numerical results tried to reproduce the experimental procedure. The acquisition frequency in the experimental tests was set to 1.4 fps and the bed height was discretized in 10 slices. The experiments show the actual position of the object in intervals of 0.71 s (1/1.4 fps), but the Monte Carlo results give the position of the object in each passing slice, independent of the time that the object remains in it. Then, the probability of an object to be at a certain height can be calculated from the Monte Carlo object trajectory using the local velocity of the object, obtained from the local dense phase velocity or the bubble velocity. In order to compare both probabilities, the experimental and the simulation, the position of the object obtained by the simulation was interpolated for each 0.71 s.

These results are shown in Figure 4.5(a) for the three simulation cases. A general good agreement between experiments and simulations and a similar tendency for the three cases can be observed. At the bottom of the bed and up to a height of 0.3 m, all the results show a similar tendency of increasing probability with height, however the simulations give a smaller value than the experimental data. On the other hand, for heights greater than 0.3 m, the experimental data shows an almost constant probability with height while the simulation data show a continuous increase. This deviation indirectly affects the values at the bottom of the bed, the results being a probability density function.

The probability of the object to attain a certain maximum depth in a cycle is plotted in Figure 4.5(b). The maximum depth attained, d_m, is presented in dimensionless form with the fixed bed height, h_{fb}, being 0 at the surface of the bed and 1 at the bottom. The previous experimental results showed a parabolic fitting which is presented in the graph. Once again, a similar tendency is observed for the simulated results, but some discrepancies are found near the bed surface. The results show a minimum of the probability around a depth of 0.3 m for all cases, with values between 0.05 and 0.08, whereas at the bottom of the bed the probability increases to values between 0.12 and 0.15. For low depths the experimental data show higher probabilities than the simulation, except for the particular case of the result for the maximum loss 2 case in the first slice, where the results are in good agreement with the experimental data.

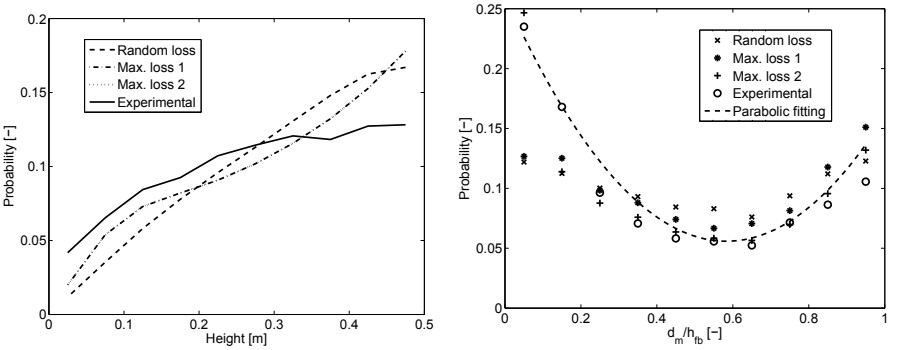

(a) (b)

Figure 4.5: Probability of (a) finding the object at a certain height and (b) attaining a determined maximum depth in a cycle.

It should be noted that the main difference between the maximum loss 2 case and the other two cases is that an object starting a rising path at the first slice is forced to reach the bed surface in the maximum loss 2 case, whereas it has a probability of 55% of remaining in the cycle for the other two cases. Therefore, it may be stated that the behaviour near the freeboard may differ from that in other regions, and thus from the mean values obtained by the model, weakening the model and causing such differences.

4.4.2 Circulation time (2-D case)

In this section, the circulation time of a neutrally-buoyant object immersed in the dense bed was calculated using the Monte Carlo results and compared with the independent experimental data measured in Soria-Verdugo *et al.* (2011). The circulation time could be calculated from the information provided by the simulated object trajectories with the addition of the time scale information. This is introduced using well-known correlations for the dense phase and bubble velocities, as established in the Monte Carlo simulation section 4.3. For all the objects simulated, the process starts in the first slice (j=1) and finishes at the freeboard, thus the circulation time is defined as the time that the object spends to complete a cycle. The statistical results for the circulation time distribution are presented using box plots. In a box plot, the distribution of the data is represented by several statistical parameters and outlying data. The data comparison was made for three experimental cases defined by the same object

and bed characteristics but a varying dimensionless gas velocities, with values of 2, 2.5 and 3. The results are plotted in Figure 4.6, comparing the previous experimental results with the data obtained for the random loss case simulation. The data of the other cases is not presented in Figure 4.6, since no significant differences were found between those cases and the random loss case.

The results obtained in the simulation were in agreement with the experimental data either for the general tendency with gas velocity and for each of the three dimensionless gas velocity cases analyzed. The simulation was run for 10^7 objects. The number of outliers of the circulation time generated for this amount of objects cannot be compared with the number of outliers obtained in the experimental data, where just 1200 cycles are observed. Therefore, no outliers were plotted for the simulation results. Instead of that, the circulation time that has the same probability as an outlier in the experimental case (1/1200) was plotted for comparison.

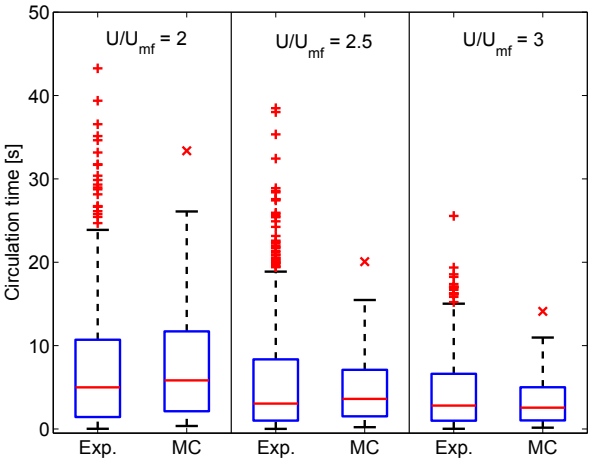

Figure 4.6: Circulation time for different U/U_{mf} in the 2-D fluidized bed.

4.4.3 Circulation time (extrapolation for a 3-D case)

In order to evaluate the validity of the 1-D model established in this work for more complex configurations, a simulation was run considering a 3-D bed. The procedure used for simulating the 3-D case is similar to that used in the 2-D case. The only difference was the equation used for the bubble diameter. The correlation of Darton (Darton *et al.*, 1977), presented in equation (4.5) was used

for the 3-D case, while Shen correlation was used for the 2-D case.

$$D_B = \frac{\left[0.54\left(U - U_{mf}\right)^{0.4}\left(h_{fb} + 4\sqrt{A_0}\right)^{0.8}\right]}{g^{0.2}} \tag{4.5}$$

where the bubble diameter, D_B, is a function of the gas velocity, U, the minimum fluidization velocity, U_{mf}, the fixed bed height, h_{fb}, the area of the distributor per number of orifices, A_0, and the gravity, g.

The results were compared with experimental data obtained in the lab-scale 3-D fluidized bed presented in section 2.2. The experimental results were obtained recording the freeboard with a zenith point of view of the camera, and then measuring the time lapse between the moment when an object disappears from the surface of the bed and the moment when it appears again on the surface. The tests were made for dimensionless gas velocities of 2 and 2.5. For a dimensionless gas velocity of 3, the object was not clearly detected in the surface due to the amount of dense phase present in the freeboard because of intense bubble eruptions.

The results of the simulations and the experiments were compared for dimensionless gas velocity of 2 and 2.5 and plotted in Figure 4.7. The simulations are shown only for the random loss case, the other two cases giving, again, very similar results. The results show a good agreement, although a wider range of dimensionless gas velocity should be analyzed. The circulation time shows a slight decrease for increasing dimensionless gas velocities, similarly to the 2-D case. The simulation for the 3-D case might therefore be considered consistent.

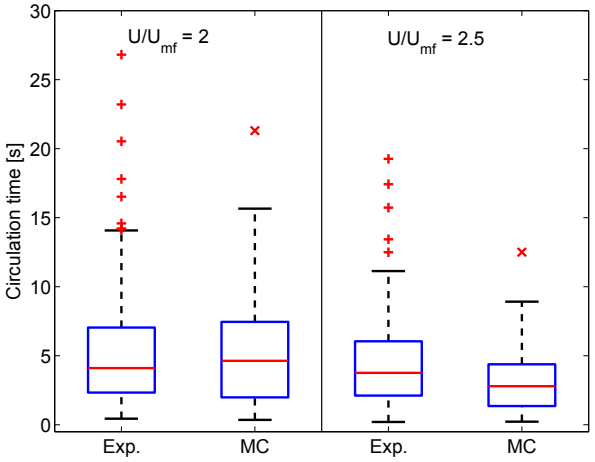

Figure 4.7: Circulation time for different U/U_{mf} in the 3-D fluidized bed.

4.5 Conclusions

In this chapter, a one dimensional model has been proposed to describe the motion of a neutrally-buoyant object in a 2-D bubbling fluidized bed for different dimensionless gas velocities. The model is based on a Monte Carlo method using three representative parameters and the results of the simulation were compared with some experimental data.

The model describes the vertical trajectories of an object inside the dense bed, using statistical parameters to simplify the complex rising and sinking processes. The sinking process is defined by the probability of an object at a certain depth to start a rising path, a parameter that is depth dependent. The rising process is characterized by the probability of a rising object to reach the bed surface in that rising path and, otherwise, its probability of stopping rising and starting a new sinking path at a given depth. These parameters can be modeled, obtained from the literature or from 2-D experiments.

The validity of the simulation was tested by comparing its results with experimental results for some independent characteristics of the object motion. With such a purpose, the probability distribution for finding an object at a certain height and the maximum depth attained by the object in a cycle were obtained experimentally and calculated from the raw experimental data. The comparison showed in both cases an overall agreement and a similar tendency with depth, while some discrepancies appeared near the bed surface.

The circulation time of an object inside the dense bed was calculated using the model results and the velocities of the object in order to introduce a time scale in the vertical trajectories. These velocities were calculated using typical correlations for the dense phase and bubble velocities in a 2-D fluidized bed. The results were compared with the experiments, showing similar values for all dimensionless gas velocities.

Finally an extrapolation for a 3-D fluidized bed was made, using the same simulation process as for the 2-D case, extrapolating the validity of the three statistical parameters that determined the sinking and rising behaviour, but employing a 3-D correlation for the bubble diameter. The comparison of the circulation time obtained by the method with the measurements showed a good agreement, similar to that obtained for the 2-D case.

Notation

A_0	Area of the distributor per number of orifices [m^2]
d	Depth in the bed (continuous variable) [m]
D_B	Bubble diameter [m]
d_j	Depth of the different slices (discrete variable) [m]
d_m	Maximum depth attained by the object [m]
g	Gravity [$m{\cdot}s^{-2}$]
h_{fb}	Fixed bed height [m]
i	Parameter that establishes at which position the object is detached in its rising path [–]
N_{jumps}	Number of jumps in a cycle [–]
N_p	Random number [–]
N_q	Random number [–]
p	Probability of an object to get the bed surface by the action of a single bubble [–]
$q\,(d)$	Probability of the object to start a rising path for a continuous depth [–]
$q\,(d_j)$	Probability of the object to start a rising path when arriving to a certain depth [–]
U	Superficial gas velocity [$m{\cdot}s^{-1}$]
U_{mf}	Minimum fluidization velocity [$m{\cdot}s^{-1}$]

References

Darton, R.C., LaNauze, R.D., Davidson, J.F. & Harrison, D. 1977 Bubble growth due to coalescence in fluidized beds. *Transactions of the Institute of Chemical Engineering* 55, 274 – 280.

Davidson, J.F. & Harrison, D. 1963 *Fluidised particles*, 1st edn. Cambridge: Cambridge University Press.

Kunii, D. & Levenspiel, O. 1991 *Fluidization Engineering*, 2nd edn. Boston: Butterworth-Heinemann.

Shen, L., Johnsson, F. & Leckner, B. 2004 Digital image analysis of hydrodynamics two-dimensional bubbling fluidized beds. *Chemical Engineering Science* 59 (13), 2607 – 2617.

Soria-Verdugo, A., Garcia-Gutierrez, L.M., Sánchez-Delgado, S. & Ruiz-Rivas, U. 2011 Circulation of an object immersed in a bubbling fluidized bed. *Chemical Engineering Science* 66 (1), 78 – 87.

CHAPTER
FIVE

Monte Carlo simulations of fuel particle motion in a 3-D large-scale fluidized bed

Contents

5.1 Introduction

In this chapter, a Monte Carlo global model was proposed to characterize the fuel particle motion throughout a large-scale 3-D bubbling fluidized bed. The model describes the global motion of a neutrally-buoyant fuel particle in the bed, analyzing its behavior both in the freeboard and inside the dense bed. The model was validated using experimental results reported in the literature of the lateral mixing of fuel particles in a large-scale 3-D bubbling fluidized bed. The

lateral displacement and the residence time, both in the freeboard and inside the dense bed, were obtained from the model. From those data, the lateral dispersion coefficient of the fuel particle was determined. The influence of the operational conditions on the lateral dispersion coefficient and on the maximum lateral distance reached by a fuel particle for different residence times in the bed, was also analyzed. Finally, an optimal distance between feeding ports, defined to ensure a suitable fuel distribution, was obtained.

5.1.1 Experimental work employed for the validation

The results obtained from the Monte Carlo model employed to characterize the motion of a fuel particle in a large-scale fluidized bed were validated with an experimental work reported in the literature by Olsson *et al.* (2012). In this section, this experimental work is described in detail since some of their characteristics were used in the model proposed in this PhD thesis.

The lateral mixing of fuel particles was analyzed in a large-scale bubbling fluidized bed. In fluidized beds, the bubble motion produces mixing vortices of dense phase particles around its preferential paths. In 3-D beds, this motion produces toroidal flows of dense phase, whose characteristics depend on the operational conditions, the pressure drop of the distributor and the characteristics of the bed material (Pallarès *et al.*, 2007). These mixing vortices generated around the bubble paths are called mixing cells and the exchange of particles between them produces the lateral mixing of particles. This phenomenon is similar for the lateral mixing behavior of a large object such as a fuel particle. The exchange of fuel particles between different mixing cells can be produced in the freeboard, during the ejection of the fuel particle by the bubbles, or inside the dense bed, as stated by Pallarès *et al.* (2007) and Olsson *et al.* (2012), following the mechanism that they defined as bubble wake mixing and emulsion drift sinking of the dense phase material. The experimental work presented by Olsson *et al.* (2012), analyzed the lateral mixing of fuel particles based on this phenomenon.

The tests were performed at ambient conditions in a bubbling fluidized bed with a cross sectional area of 1.44 m^2, with rectangular shape, in the Chalmers indirect gasifier. The bed material was silica sand particles with a density of 2600 kg/m^3 and an average particle size of 150 μm. The fixed bed height was 0.4 m, obtaining a minimum fluidization velocity of 0.02 m/s. Two dimensionless gas velocities, U/U_{mf}, were employed by the authors in the experiments: 5 and 7.5. During the tests, two types of fuel particles, wood chips

with a density of 523.5 kg/m^3 and bark pellets with a density of 1178.6 kg/m^3, were tracked. The fuel particles were covered with a phosphorescent plastic and recorded from above the bed surface using a CCTV camera at an acquisition frequency of 25 fps. Therefore, the position of the fuel particles in the plane XY over the bed surface was obtained directly from the image. The tracer particles were fed through a sampling port as a single particle or as a batch, formed by 14-20 particles. The mixing cells generated by the bubble paths are 12 in the x-direction and 5 in the y-direction, in accordance with the arrangement of the nozzles, with a rectangular shape in the cross sectional area.

Based on these experimental characteristics, the lateral mixing of fuel particles was analyzed. Olsson *et al.* (2012) calculated the lateral dispersion coefficient employing the Einstein equation (Einstein, 1956), presented here in equation (5.1):

$$D_k = \frac{\sum_{i=1}^{M} \left(\gamma_k^2/2t_c\right)_i}{M} \quad k = x, y \tag{5.1}$$

where D_k is the lateral dispersion coefficient in the k-direction, γ_k the lateral displacement in the k-direction and t_c is the global cycle time.

The mean lateral dispersion coefficient was determined for the batch experiments by averaging the individual values over a time interval between 1 and 7 min. If the fuel particle hit the walls at any moment before 7 min, just the values up to that instant were considered in order to avoid wall effects.

In addition to the lateral dispersion coefficient, other parameters were characterized experimentally by Olsson *et al.* (2012) in order to analyze the lateral mixing of fuel particles in a large-scale fluidized bed. The presence of the fuel particle at the bed surface in a time interval after the instant of its feeding to the bed was determined. The number of times that the particles were detected at the surface of each mixing cell was obtained over a time interval of 7 min employing an acquisition frequency of 25 fps. The experiments were performed for a batch of wood chips at $U/U_{mf} = 7.5$. Then, the cumulative probability of observations at the bed surface per unit of area of mixing cell was obtained. Finally, the ratio of time that a single particle of wood chip spent inside the dense bed to the total time, represented by the sum of the time inside the dense bed and in the freeboard, was determined for U/U_{mf} of 5 and 7.5. Analogously, the ratio of the lateral displacement occurring inside the dense bed to the total lateral displacement, considering together the motion inside the dense bed and in the freeboard, was also calculated for both dimensionless gas velocities.

The lateral dispersion coefficient, the cumulative probability of observa-

tions and the ratio of time and lateral displacement, obtained experimentally by Olsson *et al.* (2012), were used to validate the Monte Carlo global model proposed in this chapter.

5.2 Theoretical Model

A model based on Monte Carlo simulations is proposed to characterize the overall motion of a fuel particle in a 3-D fluidized bed. The global motion can be divided in two sub-motions: i) a motion of the fuel particle immersed in the bed and ii) a motion of the fuel particle in the freeboard. The different behaviors were studied in separated sub-models in Chapter 3 and Chapter 4, and in this chapter these sub-models were combined to generate a global model capable of describing the whole motion of fuel particles in fluidized beds.

5.2.1 Vertical motion inside the dense bed

The vertical motion of a fuel particle when it is immersed in the bed was described in detail in Chapter 4 with a 1-D Monte Carlo model. The model was based on three external parameters: i) the probability of a fuel particle to start a rising path when it is in a sinking process, $q(d)$, ii) the probability of a fuel particle to reach directly the bed surface when it starts a rising path, p, and iii) a parameter, i, that establishes the depth where the fuel particle detached from the bubble, ending its rising path prior to arrive to the bed surface. The probability of the fuel particle to start a rising path depends on the depth. This dependence was analyzed in Chapter 4 and it is presented in equation (4.1). On the other hand, the probability of a fuel particle to reach directly the bed surface was $p = 0.45$, as can be observed in the experimental results of the previous works described in Chapter 1. Finally, the assumption for the parameter i, was that the fuel particle was detached from the bubble in the position immediately before the one where the rising path started. This assumption provided a good agreement with the experimental data, as stated also in Chapter 4.

From the parameters described above, the vertical trajectory of a fuel particle for each cycle was obtained. Nevertheless, to obtain a time scale characterization, the sinking and rising velocities of the fuel particle were needed. The methodology followed to determine the sinking and the rising velocities of the fuel particle was the same than that described in previous chapters. The sinking velocity was associated with the dense phase downwards velocity using

the Kunii and Levenspiel correlation (Kunii & Levenspiel, 1991). Whereas, the fuel particle velocity in the rising path was related with 20% the mean bubble velocity as stated in Chapter 1. The bubble diameter in a 3-D fluidized bed was calculated using the Darton equation (Darton *et al.*, 1977) and the bubble velocity was obtained using the Davidson and Harrison correlation (Davidson & Harrison, 1963).

Once the velocity of the fuel particle and its vertical trajectory was determined, the circulation time needed for the fuel particle to complete a cycle inside the dense bed, was calculated. Furthermore, the maximum depth reached by the fuel particle in each cycle was also determined. Thus, the outputs of the model inside the dense bed are the circulation time and the maximum depth reached by the fuel particle in each of the N simulated cycles.

5.2.2 Freeboard motion

The motion of a fuel particle in the freeboard of the bed has been characterized for different bed conditions, dimensionless gas velocities and fixed bed heights, in Chapter 3. The fuel particle motion in the freeboard was proved to be a ballistic motion, only affected by gravity, and defined by the ejection velocity of the fuel particle, characterized by the modulus and the ejection angle, angle between the velocity direction and the vertical axis. The results obtained from the experiments carried out in Chapter 3 showed a probability function for the ejection angle expressed by an exponential distribution. The modulus of the mean ejection velocity of the fuel particle was found to be related to the mean bubble velocity times the cosine of the ejection angle. The dimensionless ratio of the modulus of the ejection velocity to the bubble velocity times the cosine of the ejection angle showed a Gaussian distribution with a mean of 1.00 and standard deviation of 0.32. These relations can be observed in equations (3.2) and (3.1) respectively, presented in Chapter 3.

Once the modulus and the ejection angle of the ejection velocity of the fuel particle were obtained, the time of flight and the lateral displacement in its ballistic motion were calculated using the ballistic equations. Those equations were formulated in Chapter 3 as equations (3.4) and (3.5).

A Monte Carlo model was developed to obtain the time of flight and the lateral displacement of a fuel particle for N cycles in the freeboard. The inputs of the simulation were the probability density function of the ejection angle and the Gaussian distribution of the relation between the modulus of the ejection velocity of the fuel particle and the bubble velocity. The outputs of the simula-

tions are N values of time of flight and lateral displacement of the fuel particle in the freeboard.

5.2.3 Global motion

The Monte Carlo sub-models for the fuel particle motion inside the dense bed and in the freeboard were combined to describe the global motion of a fuel particle in a large-scale 3-D fluidized bed using a Monte Carlo global model. Nevertheless, the lateral behavior of a fuel particle inside the dense bed was not analyzed in the previous sub-models. Therefore, new assumptions were implemented in the global model to describe the lateral motion of the fuel particle when it is immersed in the dense bed. In this way, the global motion of a fuel particle throughout the bed, both inside the dense bed and in the freeboard, was completely characterized by the Monte Carlo global model.

The lateral displacement of the fuel particle inside the dense bed was calculated based on the 3-D bed dimensions and the mixing cells distribution reported by Olsson *et al.* (2012). In this section, the procedure followed in the Monte Carlo global model to characterize the global motion of the fuel particle throughout the bed is explained.

The initial position of a fuel particle is at the surface of the bed. The fuel particle is submerged inside the dense bed, and its motion is characterized by the 1-D sub-model described in section 4.3.1 of Chapter 4. Therefore, the circulation time and the maximum depth reached by the fuel particle in a cycle were obtained. The lateral displacement of the fuel particle inside the dense bed was determined in two different cases, depending on the maximum depth reached by the fuel particle. If the maximum depth is small, the fuel particle would describe a short cycle inside the dense bed and the position where it reappears at the bed surface will be near to the position where it sank. On the other hand, if the fuel particle describes a large cycle inside the dense bed, i.e. higher depths are reached, it can reappear farther from the sinking point in the same mixing cell or even in a neighboring mixing cell.

When the maximum depth reached by the fuel particle in a cycle is lower than the mean bubble diameter at the top of the dense bed, the position where the fuel particle appears again at the bed surface is calculated from the position where it sank into the dense bed. In this case, the lateral displacement inside the dense bed would be of the order of the diameter of the bubble associated to its motion. Thus, the fuel particle emersion position was calculated using a Gaussian distribution, centered at the sinking point of the fuel particle,

and assuming that the mean bubble diameter was three times the standard deviation.

On the other hand, when the maximum depth reached by the fuel particle inside the dense bed is higher than the mean bubble diameter at the top of the dense bed, the fuel particle reappears at the bed surface in the same mixing cell than the sinking point or in a neighboring mixing cell. The probability of a fuel particle to appear in a mixing cell is inversely proportional to the distance between the center of each mixing cell and the fuel particle sinking point. Since the preferential path in a mixing cell is located at the center (Pallarès & Johnsson, 2006), the fuel particle emersion point was calculated as a Gaussian distribution centered at the center of the corresponding mixing cell, with half the lower size of the mixing cell as three times the standard deviation.

In both cases the azimuth angle was assumed to be equiprobable. Therefore, the position of the fuel particle when appearing at the bed surface is determined and the lateral displacement inside the dense bed can be calculated. The lateral displacement inside the dense bed is considered as the distance from the fuel particle sinking point to the fuel particle emersion position.

The global motion of the fuel particle in the 3-D bed was completed with the model of the fuel particle motion in the freeboard. The lateral displacement in the freeboard and the time of flight were obtained and the position where the fuel particle sank was calculated with an equiprobable azimuth angle. Therefore, the global motion of the fuel particle in a 3-D bed was completely characterized. The outputs of the global model are the positions where the fuel particle emerged and sank at the bed surface, the circulation time inside the dense bed and the time of flight in the freeboard. Thus, the displacement in a global cycle, both inside the dense bed and in the freeboard, was calculated as the distance between consecutive sinking points and the global cycle time as the sum of the circulation time and the time of flight. Finally, a number of global cycles, N, with their respective displacements and times were obtained for all the fuel particles simulated.

5.3 Results and discussion

5.3.1 Validation of the model with experimental results from the literature

The Monte Carlo global model proposed is valid for fuel particles with a neutrally-buoyant behavior, showing a proper circulation throughout the whole bed and when it is only affected in the freeboard by gravitational forces. Temperature changes and chemical reaction are not considered, so the particle properties and dimension are kept constant during the simulations. The assumptions of the sub-models and their results have been validated experimentally, as previously stated in Chapter 3 and Chapter 4. Nevertheless, the assumptions for the lateral displacement inside the dense bed and the global motion presented in section 5.2.3 were not validated previously. Therefore, in this section the results of the Monte Carlo global model were compared with the results obtained experimentally in a large-scale 3-D bubbling fluidized bed by Olsson *et al.* (2012).

Comparison of the lateral dispersion coefficient

In order to compare the results reported by Olsson *et al.* (2012) for the lateral dispersion coefficient with the results of the Monte Carlo global model, a series of simulations were carried out following the characteristics of the experimental procedure. This Monte Carlo simulations were performed using a MatLab® algorithm. The statistical distributions for the probability of starting a rising path at a certain depth, $q(d)$, the probability of reaching the bed surface directly, p, and the ejection velocity of the fuel particle were the general ones defined in previous chapters and based on 2-D experiments. On the other hand, the geometry and the characteristics of the bed and the mixing cells in the simulations were equal to the experiments reported by Olsson *et al.* (2012). The height of the bed was divided in ten slices of 0.04 m in order to characterize the vertical behavior of the fuel particle inside the dense bed. The time simulated was the same than that used in the experimental results, a time interval between 1 to 7 min corresponding to an average number of cycles, N, of 34. The wall effect was also avoided, stopping the simulation if the fuel particle hits the wall. For each cycle, the lateral dispersion coefficient was calculated according to equation (5.1) for x and y-direction, and the average in the N cycles was obtained for a fuel particle. Finally, 10^4 fuel particles were simulated in order

to obtain a representative statistical value for the lateral dispersion coefficient. The results obtained by the Monte Carlo global model are plotted in Figure 5.1 in the form of a box plot for different gas velocities, together with the experimental results obtained by Olsson *et al.* (2012) for wood chips and bark pellets. The median value, the upper and lower quartiles, corresponding with 75% and 25% of the population, and a confidence interval are given in the box plots. No outliers are depicted in order to clarify the figure.

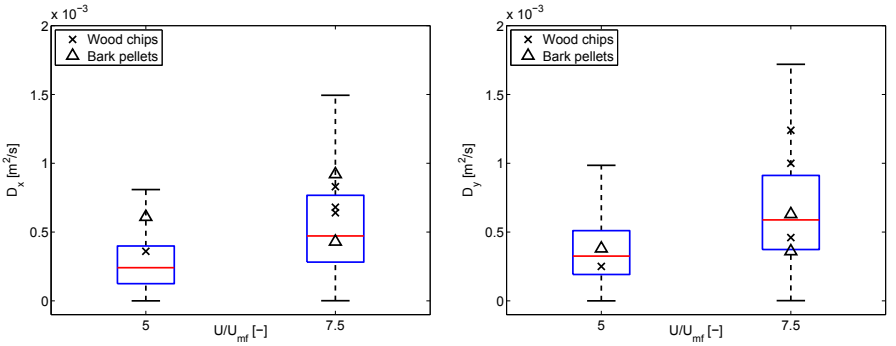

Figure 5.1: Comparison between experimental results obtained by Olsson *et al.* (2012) and results of the Monte Carlo global model for the lateral dispersion coefficient (a) in x-direction and (b) in y-direction.

Figure 5.1 shows a good agreement between the experimental data of Olsson *et al.* (2012) and the results of the Monte Carlo global model. The lateral dispersion coefficient increases with the gas velocity, since larger bubbles are produced, and thus the fluidization is more vigorous, concluding in a greater motion of the fuel particles. A small degree of anisotropy between the x-direction and y-direction was observed, being the dispersion coefficient in the y-direction higher than the x-direction because of the rectangular shape of both the bed and the mixing cells.

Comparison of the cumulative probability distribution

The presence of the fuel particle at the surface of the bed was characterized by the cumulative probability distribution of observations. The cumulative probability distribution calculated with the Monte Carlo global model was compared with the experimental values reported by Olsson *et al.* (2012). They obtained

the cumulative probability of observations experimentally for a batch of wood chips at $U/U_{mf} = 7.5$. The number of times that the fuel particles were detected at the surface of each mixing cell was obtained over a time interval of 7 min employing an acquisition frequency of 25 fps. In the simulations, a discretization with a frequency of 25 Hz was carried out in order to compare with the experimental results. Therefore, the position of a fuel particle at these discrete times were determined during 7 min and the number of times that the fuel particle was found at the surface of each mixing cell was calculated. For the comparison, 10^4 fuel particles were simulated at $U/U_{mf} = 7.5$. The cumulative probability distribution of observations per unit of mixing cell area is plotted in Figure 5.2(a) and Figure 5.2(b) obtained from the Monte Carlo global model and taken from the results reported by Olsson *et al.* (2012) respectively. The initial position of the fuel particle in the simulations is marked with a filled circle.

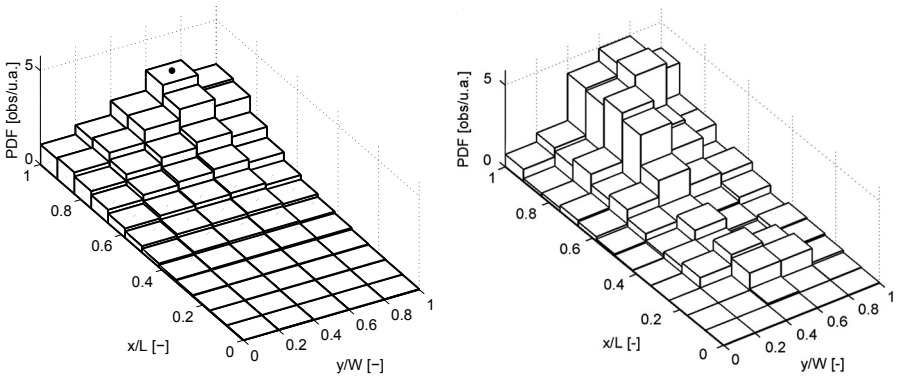

(a) (b)

Figure 5.2: Cumulative probability distribution of observations obtained from over a time interval of 7 min and $U/U_{mf} = 7.5$ (a) for the Monte Carlo global model and (b) taken directly from Olsson *et al.* (2012).

The results obtained by the Monte Carlo global model were found to be similar to the experimental results reported by Olsson *et al.* (2012). The presence of the fuel particle in the surroundings of the feeding port is higher than at farther distances. Nevertheless, for the experimental results, the presence of the fuel particle far away of the feeding port is larger. This difference can be due to the fact that the experimental data were obtained just for a batch of wood chips in 7 min in contrast of the 10^4 fuel particles simulated in the model.

Therefore, the data obtained from the experiments reported by Olsson *et al.* (2012) can be insufficient for a proper statistical result. On the other hand, in both cases, the decrement of the values in the x-direction is smoother than in the y-direction due to the rectangular shape of the bed and the mixing cells.

Comparison of the time and lateral displacement

As a final validation step, the ratio between the circulation time and the lateral displacement of a fuel particle inside the dense bed to the total of the global cycle time and the total of the global lateral displacement, both inside the dense bed and in the freeboard, were calculated for the Monte Carlo global model and compared with the experimental results reported by Olsson *et al.* (2012) for a wood chip particle. The results of the simulations were calculated for a time interval of 7 min, according to the experimental procedure. The total circulation time of a fuel particle inside the dense bed was calculated as the sum of all the circulation times inside the dense bed for each cycle, whereas the total of the global cycle time was considered as the sum of the circulation times inside the dense bed and the times of flight in the freeboard. For the lateral displacement, the ratio of the lateral displacement inside the dense bed to the total of the global lateral displacement was calculated in a similar way to the time. In order to obtain a representative statistical result, 10^4 fuel particles were simulated. The comparison between the results of the Monte Carlo global model and the experimental results is shown in Table 5.1 for two different dimensionless gas velocities.

The results of the Monte Carlo global model show a good agreement with the experimental data of Olsson *et al.* (2012) for the $U/U_{mf} = 7.5$ case. More discrepancies were observed in the case of $U/U_{mf} = 5$, which can be attributed to buoyancy effects in the wood chip particle during the experimental tests. The low ratio between the density of the wood chip and the dense bed density involved a flotsam behavior. For low dimensionless gas velocities, the buoyancy effects made the fuel particles float at the surface of the bed, increasing the time spent by the particles at the bed surface and thus decreasing the ratio t_{in}/t_{tot}. On the other hand, when the dimensionless gas velocity is increased to $U/U_{mf} = 7.5$ a more vigorous fluidization is produced, diminishing the buoyancy effects and preventing the fuel particle to float at the surface of the bed, increasing the ratio t_{in}/t_{tot}. This reduction of buoyancy effects when the dimensionless gas velocity increases has been previously reported by Wirsum *et al.* (2001) and Soria-Verdugo *et al.* (2011). The model proposed in this work

Table 5.1: Comparison of the ratio of the time and lateral displacement of the fuel particle inside the dense bed to the global values, between the Monte Carlo global model and experimental results obtained by Olsson *et al.* (2012), for $U/U_{mf} = 5$ and $U/U_{mf} = 7.5$.

$\boldsymbol{U/U_{mf} = 5}$	Model	Olsson *et al.* (2012)
t_{in}/t_{tot}	0.989 ($\kappa = \pm 0.002$)	0.60 ($\kappa = \pm 0.023$)
L_{in}/L_{tot}	0.721 ($\kappa = \pm 0.043$)	0.55 ($\kappa = \pm 0.08$)

$\boldsymbol{U/U_{mf} = 7.5}$	Model	Olsson *et al.* (2012)
t_{in}/t_{tot}	0.979 ($\kappa = \pm 0.002$)	0.97 ($\kappa = \pm 0.014$)
L_{in}/L_{tot}	0.664 ($\kappa = \pm 0.002$)	0.78 ($\kappa = \pm 0.026$)

considers fuel particles with a neutrally-buoyant behavior and thus, the discrepancies were more important for the case of $U/U_{mf} = 5$ when buoyancy effects were significant.

From the results of this section it can be concluded that the results of the Monte Carlo global model and the experimental results reported by Olsson *et al.* (2012) showed a general good agreement for neutrally-buoyant objects. Therefore, the Monte Carlo global model proposed describes accurately the fuel particle behavior in a 3-D fluidized bed.

5.3.2 Determination of the lateral dispersion coefficient for different gas velocities

Once the Monte Carlo global model was validated with experimental data, several other results were obtained from the simulations. The geometry of the bed and mixing cells employed for these results are still those of the experimental facility described by Olsson *et al.* (2012). In this section, new simulations were performed in order to study the influence of the bed walls on the values of the lateral dispersion coefficient, and its variation with the dimensionless gas velocity. The convergence of the results as a function with the time considered for the simulations was also analyzed.

Figure 5.3 shows the variation of the mean value of the lateral dispersion

coefficient with the number of global cycles considered for a fuel particle simulated with the Monte Carlo global model, using a dimensionless gas velocity of 5. The lateral dispersion coefficient in the x-direction, D_x, the y-direction, D_y, and the radial direction, D_r, were calculated for two different configurations: with bed limits maintaining the dimensions of the experimental facility reported by Olsson *et al.* (2012), (Figure 5.3(a)), and for a similar configuration without walls, (Figure 5.3(b)).

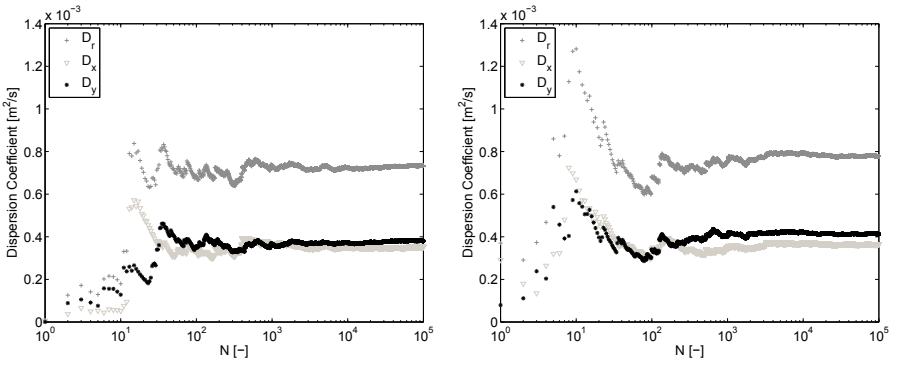

(a) (b)

Figure 5.3: Variation of the mean value of lateral dispersion coefficients D_x, D_y and D_r, for a configuration (a) with the fluidized bed dimensions reported by Olsson *et al.* (2012) and (b) for a similar configuration without walls, for $U/U_{mf} = 5$.

The values of the lateral dispersion coefficients are slightly lower in the case with walls (Figure 5.3(a)) than in the case without bed limits (Figure 5.3(b)), due to the hits of the fuel particles with the bed limits. Furthermore, the differences between the lateral dispersion coefficient in the x and y-direction are higher when removing the walls in the simulations because of the larger influence of the rectangular shape of the mixing cells. The lateral dispersion coefficients show scattering for low numbers of global cycles, nevertheless a constant value was reached for high numbers of cycles. The number of cycles needed in the simulations to obtain a constant value of lateral dispersion coefficients was above 10^4 global cycles, as can be observed in Figure 5.3. This number of global cycles is much higher than that employed in the simulations carried out for the experimental comparison, just 34 cycles, obtaining in that case a higher dispersion in the values (see Figure 5.1). In order to study the effect of the number of cycles, i.e. the time considered, on the scattering of the lateral

dispersion coefficient, 10^5 fuel particles were analyzed.

The limits of the scattering of the lateral dispersion coefficient in the radial direction are shown in Figure 5.4 as a function of the number of global cycles for a dimensionless gas velocity of 5. The limits represent the fitting of the maximum and minimum values of the lateral dispersion coefficient obtained for 10^5 fuel particles simulated, with an average cycle time equal to 13 s. The scattering found in the literature for the lateral dispersion coefficient might be attributed to the effect of the time considered in the calculation or in the measurements. As can be observed in Figure 5.4, the lateral dispersion coefficient varied between 10^{-8} and 10^{-2} m^2/s for short times in the case of a dimensionless gas velocity of 5. The range of variation diminished when increasing the time considered. Nevertheless, the mean value of the lateral dispersion coefficient is uniform with the number of cycles considered.

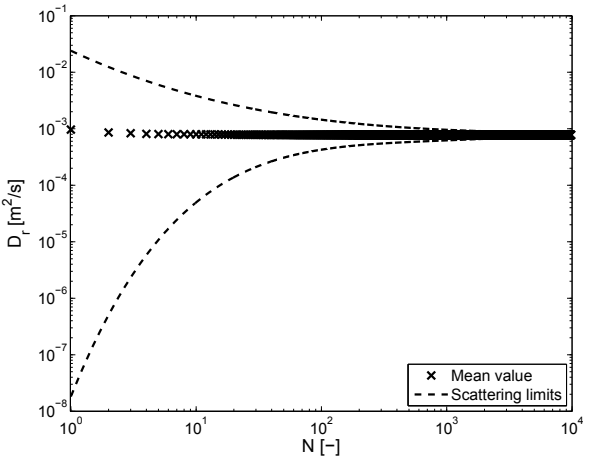

Figure 5.4: Scattering and mean value of the lateral dispersion coefficient in the radial direction as a function of the number of global cycles, for a configuration without walls and $U/U_{mf} = 5$.

The influence of the dimensionless gas velocity in the lateral dispersion coefficient in the radial direction was also analyzed in the simulations. The value of U/U_{mf} was varied from 2 to 8 for the general configuration without bed limits. The statistical distribution of the lateral dispersion coefficient is presented in Figure 5.5(a) in the form of a box plot for just one fuel particle with 10^5 global cycles at different U/U_{mf}. No outliers are depicted in the figure for clarifying purposes. The mean value of the distribution is also plotted in Figure 5.5(a) marked with a cross. Figure 5.5(b) shows the mean and median values of the

lateral dispersion coefficient and the fitting for both values, as a function of the dimensionless gas velocities.

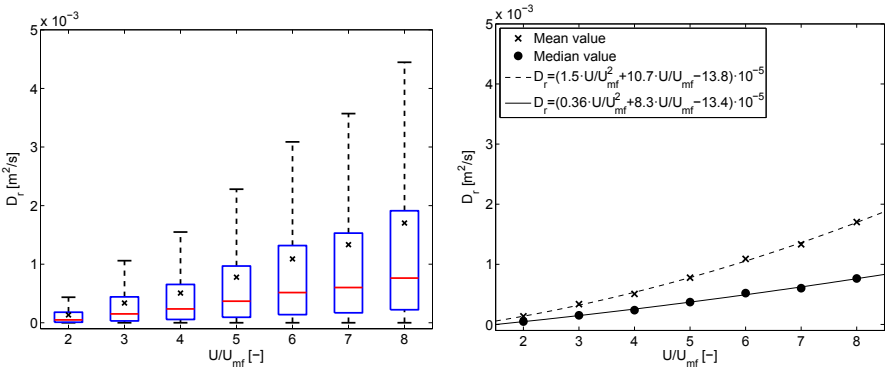

(a) (b)

Figure 5.5: Lateral dispersion coefficient in radial direction (a) distribution in a box plot and (b) mean and median values with a parabolic fitting, obtained with the Monte Carlo global model for different U/U_{mf}.

An increment in the dimensionless gas velocity involves a higher lateral dispersion coefficient, as can be observed in Figure 5.5(a). The scattering of the lateral dispersion coefficient also increases with the dimensionless gas velocity. The increase of the lateral dispersion coefficient of a fuel particle with the gas velocity is in accordance with the results already reported in the literature by several authors (Salam *et al.*, 1987; Pallarès & Johnsson, 2006; Pallarès *et al.*, 2007). The increase of the mean and median values of the lateral dispersion coefficient with the dimensionless gas velocity is parabolic, as can be seen in Figure 5.5(b). Determination coefficients R^2 of 0.997 and 0.994 was obtained for the parabolic fitting of the mean and median values respectively. The maximum discrepancies of the mean and median values of the lateral dispersion coefficient for 100 fuel particles is lower than 1.6% and 2.3% respectively for all the dimensionless gas velocities.

5.3.3 Characterization of the feeding ports distance for different configurations

The location of the feeding ports in a fluidized bed reactor is a key parameter in order to obtain a homogenous thermal conversion of the fuel particle

in the bed, avoiding the formation of hot or cold spots. The optimal location and number of the feeding ports is defined when the fuel particles can be distributed homogenously in the whole bed. An optimal distribution of the feeding ports would produce higher thermal conversion efficiency and a reduction of the maintenance costs.

The residence time of the fuel particle in the bed is another key parameter in the performance of fluidized bed reactors, and thus it should be considered in the determination of the feeding ports location. This residence time can be associated to the time in which the devolatilization process of a fuel particle occurs. The motion of the fuel particle in the bed during the devolatilization process involves different mixing behaviors described by the Damköhler number. The Damköhler number is defined, for horizontal processes, as the ratio of the lateral transport time to the thermal conversion time of a fuel particle, defined in equation (1.5). High ratios between lateral dispersion and devolatilization times, described by a high Damköhler number, means that the reaction dominates and the fuel particle thermal conversion occurs close to the feeding ports, with a poor distribution through the whole bed. On the other hand, when the dispersion time is much lower than the devolatilization time (low Damköhler numbers), the lateral transport mechanism dominates and the fuel particle is properly distributed over the bed prior to its thermal conversion (Gómez-Barea & Leckner, 2010). Several authors have determined experimentally the devolatilization times of biomass fuel particles as a function of size and shape. Wang *et al.* (2005) and de Diego *et al.* (2002) obtained devolatilization times between 20 and 250 s for wood fuels of different sizes, while for Sreekanth *et al.* (2008) the values range between 50 and 350 s also for wood particles.

In this section, simulations were performed to study the maximum lateral displacement for different number of global cycles and dimensionless gas velocities, employing the Monte Carlo global model. The global time employed in each simulation varied from 30 to 360 s in intervals of 30 s, according to the devolatilization times reported in the literature. The different dimensionless gas velocities simulated were 2, 4, 6 and 8. Four different configurations were considered in the simulations, one of them without bed limits and the other three using the bed geometry reported by Olsson *et al.* (2012), but varying the initial position of the fuel particle in the simulations, as showed in Figure 5.6.

The total number of fuel particles simulated was 10^4 for each configuration, devolatilization time, t_{dev}, and dimensionless gas velocity, U/U_{mf}. The distance between the farther position reached by the fuel particle and the injec-

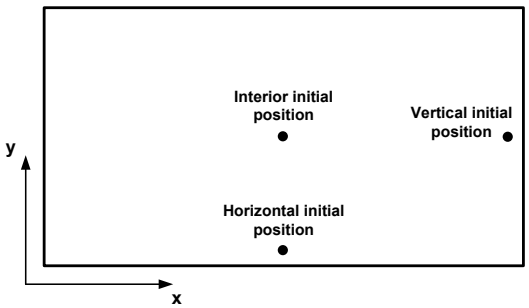

Figure 5.6: Scheme of the initial position for the different configurations of the bed with walls.

tion point was calculated for different devolatilization times and gas velocities. The optimal distance between feeding ports was estimated as two times the median value of the largest distance calculated for the 10^4 fuel particles. In Figure 5.7 the optimal feeding ports distance is plotted as a function of the devolatilization time, for all the dimensionless gas velocities and configurations.

The optimal distance between feeding ports increases with the dimensionless gas velocity and the devolatilization time for all the configurations because of the larger lateral displacement of the fuel particle. This increment of the optimal feeding ports distance depends on the position of the feeding ports. For the dimensions of the bed simulated, where the distance between the horizontal walls (y-direction) was smaller than the distance between the vertical walls (x-direction), the results vary. For devolatilization times up to 90 s, the variation of the optimal feeding ports distance is similar for all the configurations. After that instant, for the vertical and interior configurations, the increment of the optimal feeding ports distance with U/U_{mf} is smoother than in the case of the horizontal initial position or the case without walls. This smoother increment shall be attributed to the hits of the fuel particle with the horizontal bed limits in the vertical and interior configurations, whereas the bed limits are farther to the initial position for the horizontal configuration. In the results of the configuration without bed limits no changes in the variation of the optimal feeding ports distance are observed for the range of devolatilization times simulated, as can be seen in Figure 5.7(d). The optimal distance between feeding ports for the horizontal configuration is quite similar to the case without walls, showing differences just for high devolatilization times and gas velocities when the lateral displacement of the fuel particle is comparable to the distance to the walls.

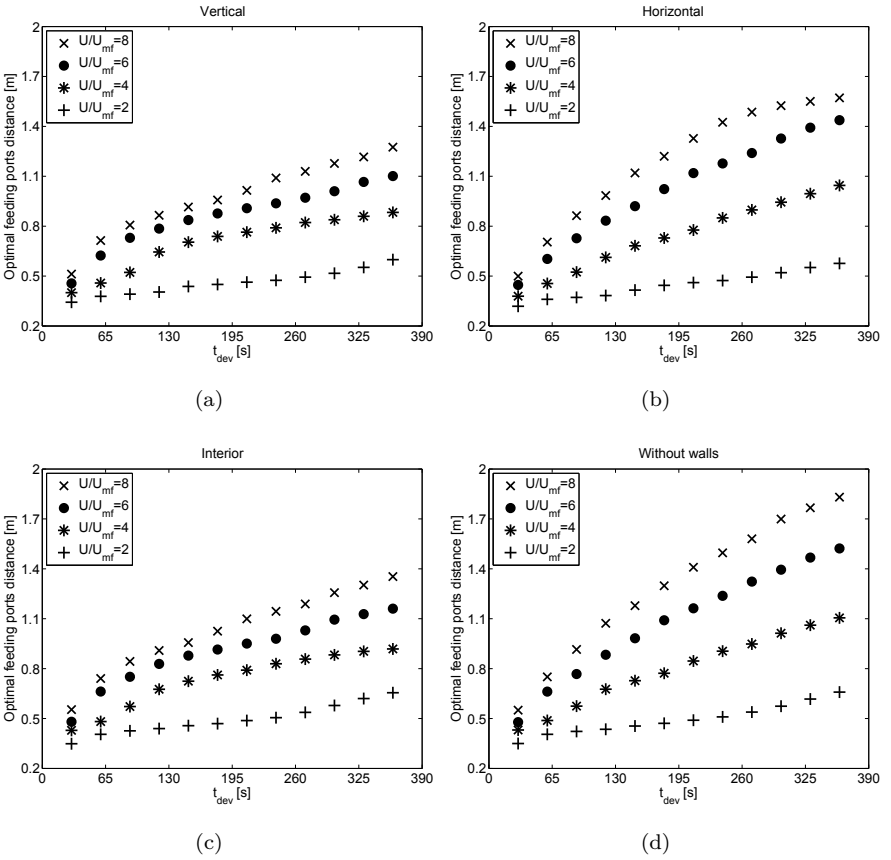

Figure 5.7: Optimal feeding ports distance as a function of the devolatilization time, for different U/U_{mf} (a) vertical initial position, (b) horizontal initial position, (c) interior initial position and (d) without walls configuration.

Finally, the results of the optimal feeding ports distance reported in Figure 5.7 could be employed to determine the optimal number of feeding ports for a particular bed geometry.

5.4 Conclusions

In this chapter a model based on a Monte Carlo method was developed to describe the global motion of a neutrally-buoyant fuel particle in a large scale 3-D fluidized bed. The global motion was divided in two sub-motions, the motion when the fuel particle is immersed in the bed and the motion in the freeboard.

The outputs of the Monte Carlo global model were the lateral displacement of the fuel particle, the circulation time of the fuel particle inside the dense bed and the time of flight in the freeboard. The results obtained from the Monte Carlo global model were compared with experimental results reported in the literature. The lateral dispersion coefficient, the distribution of the fuel particle throughout the surface of the bed, and the ratio of the circulation time and the lateral displacement of fuel particle inside the dense bed to the global cycle time and global lateral displacement were compared with the experimental data, showing a general good agreement. This provide an experimental validation of the model for a 3-D bed.

The influence of the gas velocity on the lateral dispersion coefficient was also analyzed in the simulations of the Monte Carlo global model. The lateral dispersion coefficient was calculated for several dimensionless gas velocities between 2 and 8, showing an increment of the lateral dispersion coefficient with the dimensionless gas velocity, in accordance with the literature. The increase of the mean and median values of the lateral dispersion coefficient with the gas velocity followed a parabolic tendency with a high determination coefficient R^2 associated to the fitting. The time considered in the determination of the lateral dispersion coefficient affects the scattering obtained, being higher for shorter times. This scattering is also larger for high dimensionless gas velocities.

The maximum distance reached by a fuel particle from the feeding ports was also obtained for different gas velocities and residence times. From this parameter, the optimal distance between feeding ports was calculated for several configurations, varying the feeding ports location. The residence time of a fuel particle in the bed was associated with the devolatilization times of fuel particles to determine the optimal feeding ports distance for each configuration as a function of the dimensionless gas velocities. For higher dimensionless gas velocities and devolatilization times the optimal distance between feeding ports was larger. The influence of the bed limits on the optimal location of the feeding ports was analyzed, obtaining a reduction of the distance between feeding ports when the bed walls are closer. Finally, for a particular bed geometry, the optimal number and location of feeding ports to guarantee a proper distribution of fuel particles throughout the bed can be calculated from the results presented in this work.

Notation

D_k	Lateral dispersion coefficient in the k-direction [$m^2 \cdot s^{-1}$]
D_r	Lateral dispersion coefficient in the radial direction [$m^2 \cdot s^{-1}$]
D_x	Lateral dispersion coefficient in x-direction [$m^2 \cdot s^{-1}$]
D_y	Lateral dispersion coefficient in y-direction [$m^2 \cdot s^{-1}$]
L_{in}	Total lateral displacement inside the dense bed [m]
L_{tot}	Total of the global lateral displacement in the bed [m]
N	Number of cycles simulated [−]
p	Probability of a fuel particle to get the bed surface by the action of a single bubble [−]
$q(d)$	Probability of a fuel particle to start a rising path for a continuous depth [−]
t_c	Global cycle time [s]
t_{dev}	Devolatilization time [s]
t_{in}	Total circulation time of the fuel particle inside the dense bed [s]
t_{tot}	Total of the global cycle time of the fuel particle in the bed [s]
U	Superficial gas velocity [$m \cdot s^{-1}$]
U_{mf}	Minimum fluidization velocity [$m \cdot s^{-1}$]
γ_k	Lateral displacement in k-direction [m]
κ	Maximum error [-]

References

Darton, R.C., LaNauze, R.D., Davidson, J.F. & Harrison, D. 1977 Bubble growth due to coalescence in fluidized beds. *Transactions of the Institute of Chemical Engineering* 55, 274 – 280.

Davidson, J.F. & Harrison, D. 1963 *Fluidised particles*, 1st edn. Cambridge: Cambridge University Press.

de Diego, L.F., García-Labiano, F., Abad, A., Gayán, P. & Adánez, J. 2002 Modeling of the devolatilization of nonspherical wet pine wood particles in fluidized beds. *Industrial & Engineering Chemistry Research* 41 (15), 3642 – 3650.

Einstein, A. 1956 Investigations on the theory of the brownian movement. *Dover Publications, Inc* .

Gómez-Barea, A. & Leckner, B. 2010 Modeling of biomass gasification in fluidized bed. *Progress in Energy and Combustion Science* 36 (4), 444 – 509.

Kunii, D. & Levenspiel, O. 1991 *Fluidization Engineering*, 2nd edn. Boston: Butterworth-Heinemann.

Olsson, J., Pallarès, D. & Johnsson, F. 2012 Lateral fuel dispersion in a large-scale bubbling fluidized bed. *Chemical Engineering Science* 74 (0), 148 – 159.

Pallarès, D., Díez, P & Johnsson, F. 2007 Experimental analysis of fuel mixing patterns in a fluidized bed. In *The 12th International Conference on Fluidization - New Horizons in Fluidization Engineering*, pp. 929 – 936.

Pallarès, D. & Johnsson, F. 2006 A novel technique for particle tracking in cold 2-dimensional fluidized beds - simulating fuel dispersion. *Chemical Engineering Science* 61 (8), 2710 – 2720.

Salam, T.F., Ren, Y. & Gibbs, B.M. 1987 Lateral solid and thermal dispersion in fluidized bed combustors. In *9th International Conference on Fluidized Bed Combustion*, pp. 541 – 545.

Soria-Verdugo, A., Garcia-Gutierrez, L.M., García-Hernando, N. & Ruiz-Rivas, U. 2011 Buoyancy effects on objects moving in a bubbling fluidized bed. *Chemical Engineering Science* 66 (12), 2833 – 2841.

Sreekanth, M., Sudhakar, D.R., Prasad, B.V.S., Kolar, A.K. & Leckner, B. 2008 Modelling and experimental investigation of devolatilizing wood in a fluidized bed combustor. *Fuel* 87 (12), 2698 – 2712.

Wang, X., Kersten, S.R.A., Prins, W. & van Swaaij, W.P.M. 2005 Biomass pyrolysis in a fluidized bed reactor. part 2: Experimental validation of model results. *Industrial & Engineering Chemistry Research* 44 (23), 8786 – 8795.

Wirsum, M., Fett, F., Iwanowa, N. & Lukjanow, G. 2001 Particle mixing in bubbling fluidized beds of binary particle systems. *Powder Technology* 120, 63 – 69.

CHAPTER
SIX

Conclusions

In this dissertation, a model of the motion of a large object with a neutrally-buoyant behavior throughout a bubbling fluidized bed has been performed. The model is based on parameters obtained from an experimental characterization. The measured elemental parameters of the object motion are characterized by their statistical distributions. The model relies on the simulation of the relation between such statistical distributions, using a Monte Carlo method.

This PhD thesis is a fundamental study, but the results obtained can be directly applied for the design and characterization of fluidized bed reactors. The information obtained referring to the motion of objects throughout the bed has been used to determine the lateral dispersion coefficient of a fuel particle in a large-scale bubbling fluidized bed. This is a basic parameter for the determination of the proper feeding ports location and operational conditions of a fluidized bed reactor. Also, the model allows to calculate the time intervals when the objects are in the freeboard or remains immersed in the dense bed. These periods of time can be compared with the characteristic fuel conversion times.

The motion of the object has been modeled using different sub-models according to the different dynamics present in the bed. These dynamics include the motion in the freeboard, based on the ejection velocity and gravity, the sinking motion inside the dense bed, based on the dense phase motion, and the rising motion inside the dense bed, based on object-bubble interactions. Each sub-model has been tested and validated independently, and then merged together and validated as a complete unit.

The experiments were carried out in a 2-D facility with optical access to the bed and in a 3-D lab-scale bubbling fluidized bed where zenith images were acquired. The characterization of the object motion employed two different measurement techniques, based on digital image analysis. In the first one, the object emits a green light and it is detected in complete darkness. In the second

one, specially developed for this thesis, the position of the object is acquired together with that of the dense phase, so the relative position of bubbles and the surface of the bed is obtained. Both techniques allowed to determine the object position at each instant, and thus the trajectory and velocity of the object in the 2-D bed. In the 3-D bed, only the object position when appearing at the surface was recorded.

The first study in this dissertation deals with the object motion in the freeboard. For large objects, the gas drag force is not relevant and interactions with the dense phase can be neglected, so the object motion can be described as ballistic, relying only on the velocity vector when the object is ejected to the freeboard and the gravitational force. The experiments confirmed these assumptions. The ejection velocity obtained experimentally showed statistical distributions for both angle and modulus. The ejection angle showed an exponential probability distribution, diminishing the probability from low ejection angles, around the vertical direction, to higher ones. The modulus of the object ejection velocity showed a mean value equal to the mean bubble velocity times the cosine of the ejection angle, and a Gaussian probability distribution around that value. This result is also valid for different gas velocities and bed heights. A model based on the ballistic behavior and Monte Carlo simulations considering the probability distributions of the ejection velocity was developed. The time of flight of the object and its lateral displacement during the object motion in the freeboard were obtained directly from the tests and compared with the model results for validation. A dimensionless form of the time of flight and the lateral displacement were proposed as a function of the mean bubble velocity, in order to compare different cases of bed dynamics. The dimensionless form of the probability density function showed a Gaussian distribution for the time of flight and an exponential distribution for the lateral displacement. A comparison on the distributions of time of flight and lateral displacement between the experimental results and the Monte Carlo simulations in dimensionless form showed a very good agreement between cases for different dimensionless gas velocities. As a general result of this study, the time of flight and the lateral displacement can be determined from the dimensionless form proposed, as a function of the mean bubble velocity with three different degrees of accuracy: i) a median value, for the dimensionless forms of both time and lateral dispersion equal to unity; ii) probability distributions of time and lateral dispersion using the representative parameters obtained for the Gaussian and exponential probability density function; and iii) a result obtained running the simulations

of the Monte Carlo model.

The second study concerned the modeling of the vertical motion (1-D model) of an object inside the dense bed. Objects were considered to have a neutrally-buoyant behavior. The characterization of the 1-D motion relied on experimental evidence presented in previous works. Experiments obtained prior to this PhD thesis, but with the participation of its author, were used as a source of input data and for comparison and validation. The model rely on three main parameters: i) the probability of a rising object to reach directly the surface of the bed; ii) the probability of a sinking object to start a rising process at a certain position; and iii) if that first case is not fulfilled, the position where the object was detached from the bubble in its rising path. The first probability was obtained experimentally in previous works for a number of bed and particle configurations, obtaining a constant value of 45%. The second one was obtained experimentally in this thesis for an object with a neutrally-buoyant behavior. A model based on Monte Carlo simulations employing these parameters and information on the object mean sinking and rising velocities was developed. The results of the model are the distribution of the circulation time of the object in a cycle, i.e. the lapse between starting a sinking path at the bed surface and coming back to it, and the probability of the maximum depth attained by an object in a cycle. The simulation results were compared with the experimental data showing a good agreement. Finally, the model was extrapolated to calculate the circulation time for a 3-D bed, and the results were compared with experimental data obtained in a lab-scale 3-D bubbling fluidized bed. The comparison of the results for the 3-D bed showed also a good agreement.

The last study in this PhD thesis consisted of the development of a global model from the two previous sub-models. The results were presented as an application to characterize the motion of a fuel particle in a 3-D large-scale fluidized bed. Nevertheless, a simple combination of the two sub-models lacked some features that should be defined and modeled. A relevant motion, the lateral behavior of the fuel particle when it is inside the dense bed, was not addressed in the previous sub-models. Therefore, the model was extended considering an assumption based on literature evidence. The fuel particle was considered to move in the lateral direction inside the dense bed with some conditions based on the well-established mixing cell structure, the bubble diameter and the maximum depth attained by the object in a cycle inside the dense bed. With these assumptions, the model is complete and could deliver information on the global motion and lateral displacement versus time. The

results of the model were validated in comparison with experimental data on the fuel dispersion in a large-scale fluidized bed available in the literature. The validation showed a good agreement between the Monte Carlo simulations and the experimental results. The lateral dispersion coefficient of a fuel particle was calculated for a wide range of dimensionless gas velocities. The mean lateral dispersion coefficient showed a smooth parabolic tendency for increasing gas velocity. Finally, the maximum lateral distance reached by a fuel particle was obtained for a time scale associated to the devolatilization time of the fuel particle, for different gas velocities and varying the initial position of the fuel particle in the simulations. This maximum distance reached by the fuel particle can be used for design criteria on the optimal location of the feeding ports in fluidized bed reactors, in order to ensure a proper distribution of the fuel particles. Therefore, an optimal distance between feeding ports was proposed for a wide range of devolatilization times, different locations of the feeding ports and several gas velocities.

Alphabetical list of references

Almendros-Ibáñez, J.A., Sobrino, C., de Vega, M. & Santana, D. 2006 A new model for ejected particle velocity from erupting bubbles in 2-D fluidized beds. *Chemical Engineering Science* 61 (18), 5981 – 5990.

Bai, W., Keller, N.K.G., Heindel, T.J. & Fox, R.O. 2013 Numerical study of mixing and segregation in a biomass fluidized bed. *Powder Technology* 237 (0), 355 – 366.

Bi, J., Yang, G. & Kojima, T. 1995 Lateral mixing of coarse particles in fluidized beds of fine particles. *Chemical Engineering Research and Design* 73, 162–167.

Bruni, G., Solimene, R., Marzocchella, A., Salatino, P., Yates, J.G., Lettieri, P. & Fiorentino, M. 2002 Self-segregation of high-volatile fuel particles during devolatilization in a fluidized bed reactor. *Powder Technology* 128 (1), 11 – 21.

Caicedo, G.R., Ruiz, M.G., Marqués, J.P. & Soler, J.G. 2002 Minimum fluidization velocities for gas-solid 2D beds. *Chemical Engineering and Processing: Process Intensification* 41 (9), 761 – 764.

Darton, R.C., LaNauze, R.D., Davidson, J.F. & Harrison, D. 1977 Bubble growth due to coalescence in fluidized beds. *Transactions of the Institute of Chemical Engineering* 55, 274 – 280.

Davidson, J.F. & Harrison, D. 1963 *Fluidised particles*, 1st edn. Cambridge: Cambridge University Press.

de Diego, L.F., García-Labiano, F., Abad, A., Gayán, P. & Adánez, J. 2002 Modeling of the devolatilization of nonspherical wet pine wood particles in fluidized beds. *Industrial & Engineering Chemistry Research* 41 (15), 3642 – 3650.

Einstein, A. 1956 Investigations on the theory of the brownian movement. *Dover Publications, Inc* .

Fiorentino, M., Marzocchella, A. & Salatino, P. 1997 Segregation of fuel particles and volatile matter during devolatilization in a fluidized bed reactor-II. Experimental. *Chemical Engineering Science* 52 (12), 1909 – 1922.

Fung, A.S. & Hamdullahpur, F. 1993 A gas and particle flow model in the freeboard of a fluidized bed based on bubble coalescence. *Powder Technology* 74 (2), 121 – 133.

Geldart, D. 1973 Types of gas fluidization. *Powder Technology* 7 (5), 285 – 292.

Geldart, D. & Baeyens, J. 1985 The design of distributors for gas-fluidized beds. *Powder Technology* 42 (1), 67 – 78.

Geldart, D. & Cranfield, R.R. 1972 The gas fluidisation of large particles. *The Chemical Engineering Journal* 3 (0), 211 – 231.

Gómez-Barea, A. & Leckner, B. 2010 Modeling of biomass gasification in fluidized bed. *Progress in Energy and Combustion Science* 36 (4), 444 – 509.

Hernández-Jiménez, F., Third, J.R., Acosta-Iborra, A. & Müller, C.R. 2011 Comparison of bubble eruption models with two-fluid simulations in a 2d gas-fluidized bed. *Chemical Engineering Journal* 171 (1), 328 – 339.

Ito, O., Kawabe, R., Miyamoto, T., Orita, H., Mizumoto, M., Miyadera, H., Tomuro, J., Hokari, N. & Iwase, T. 1999 Direct measurement of particle motion in a large-scale FBC boiler model. In *International Conference on Fluidized Bed Combustion*, p. 217.

Karri, S.B.R. & Werther, J. 2003 *Handbook of fluidization and fluid-particle systems*. New York: Marcel Dekker Inc.

Kunii, D. & Levenspiel, O. 1991 *Fluidization Engineering*, 2nd edn. Boston: Butterworth-Heinemann.

Leckner, B., Szentannai, P. & Winter, F. 2011 Scale-up of fluidized-bed combustion - a review. *Fuel* 90 (10), 2951 – 2964.

Leckner, B. & Werther, J. 2000 Scale-up of circulating fluidized bed combustion. *Energy & Fuels* 14 (6), 1286 – 1292.

Lim, K.S. & Agarwal, P.K. 1994 Circulatory motion of a large and lighter sphere in a bubbling fluidized bed of smaller and heavier particles. *Chemical Engineering Science* 49 (3), 421 – 424.

Müller, C.R., Davidson, J.F., Dennis, J.S. & Hayhurst, A.N. 2007 A study of the motion and eruption of a bubble at the surface of a two-dimensional fluidized bed using particle image velocimetry (PIV). *Industrial & Engineering Chemistry Research* 46 (5), 1642 – 1652.

Nguyen, T.H. & Grace, J.R. 1978 Forces on objects immersed in fluidized beds. *Powder Technology* 19 (2), 255 – 264.

Nienow, A.W., Rowe, P.N. & Chiba, T. 1978 Mixing and segregation of a small portion of large particles in gas fluidized beds of considerably smaller ones. *AIChe Symposium Series* 74, 45 – 53.

Olsson, J., Pallarès, D. & Johnsson, F. 2012 Lateral fuel dispersion in a large-scale bubbling fluidized bed. *Chemical Engineering Science* 74 (0), 148 – 159.

Pallarès, D., Díez, P & Johnsson, F. 2007 Experimental analysis of fuel mixing patterns in a fluidized bed. In *The 12th International Conference on Fluidization - New Horizons in Fluidization Engineering*, pp. 929 – 936.

Pallarès, D. & Johnsson, F. 2006 A novel technique for particle tracking in cold 2-dimensional fluidized beds - simulating fuel dispersion. *Chemical Engineering Science* 61 (8), 2710 – 2720.

Rees, A.C., Davidson, J.F., Dennis, J.S. & Hayhurst, A.N. 2005 The rise of a buoyant sphere in a gas-fluidized bed. *Chemical Engineering Science* 60 (4), 1143 – 1153.

Rios, G. M., Dang Tran, K. & Masson, H. 1986 Free object motion in a gas fluidized bed. *Chemical Engineering Communications* 47 (4-6), 247 – 272.

Salam, T.F., Ren, Y. & Gibbs, B.M. 1987 Lateral solid and thermal dispersion in fluidized bed combustors. In *9th International Conference on Fluidized Bed Combustion*, pp. 541 – 545.

Sánchez-Delgado, S., Almendros-Ibáñez, J.A., García-Hernando, N. & Santana, D. 2011 On the minimum fluidization velocity in 2D fluidized beds. *Powder Technology* 207, 145 – 153.

Sánchez-Delgado, S., Marugán-Cruz, C., Soria-Verdugo, A. & Santana, D. 2013 Estimation and experimental validation of the circulation time in a 2D gas-solid fluidized beds. *Powder Technology* 235, 669 – 676.

Santana, D., Nauri, S., Acosta, A., García, N. & Macías-Machín, A. 2005 Initial particle velocity spatial distribution from 2-D erupting bubbles in fluidized beds. *Powder Technology* 150 (1), 1 – 8.

Shen, L., Johnsson, F. & Leckner, B. 2004 Digital image analysis of hydrodynamics two-dimensional bubbling fluidized beds. *Chemical Engineering Science* 59 (13), 2607 – 2617.

Soria-Verdugo, A. 2010 Motion of objects immersed in a bubbling fluidized bed. PhD thesis, Carlos III University of Madrid.

Soria-Verdugo, A., Garcia-Gutierrez, L.M., García-Hernando, N. & Ruiz-Rivas, U. 2011*a* Buoyancy effects on objects moving in a bubbling fluidized bed. *Chemical Engineering Science* 66 (12), 2833 – 2841.

Soria-Verdugo, A., Garcia-Gutierrez, L.M., Sánchez-Delgado, S. & Ruiz-Rivas, U. 2011*b* Circulation of an object immersed in a bubbling fluidized bed. *Chemical Engineering Science* 66 (1), 78 – 87.

Soria-Verdugo, A., García-Hernando, N., Almendros-Ibáñez, J.A. & Ruiz-Rivas, U. 2011*c* Motion of a large object in a bubbling fluidized bed with a rotating distributor. *Chemical Engineering and Processing: Process Intensification* 50 (8), 859 – 868.

Sreekanth, M., Sudhakar, D.R., Prasad, B.V.S., Kolar, A.K. & Leckner, B. 2008 Modelling and experimental investigation of devolatilizing wood in a fluidized bed combustor. *Fuel* 87 (12), 2698 – 2712.

Wang, X., Kersten, S.R.A., Prins, W. & van Swaaij, W.P.M. 2005 Biomass pyrolysis in a fluidized bed reactor. part 2: Experimental validation of model results. *Industrial & Engineering Chemistry Research* 44 (23), 8786 – 8795.

Wirsum, M., Fett, F., Iwanowa, N. & Lukjanow, G. 2001 Particle mixing in bubbling fluidized beds of binary particle systems. *Powder Technology* 120, 63 – 69.

Xiang, Q., Huang, G., Ni, M., Cen, K. & Tao, T. 1987 Lateral dispersion of large coal particles in an industrial scale fluidised bed combustor. In *9th International Conference on Fluidized Bed Combustion*, pp. 546 – 553.

Xiao, P., Yan, G. & Wang, D. 1998 Investigation on horizontal mixing of particles in dense bed in circulating fluidized bed (CFB). *Journal of Thermal Science* 7 (2), 78 – 84.

Zhang, Y., Jin, B. & Zhong, W. 2009 Experimental investigation on mixing and segregation behavior of biomass particle in fluidized bed. *Chemical Engineering and Processing: Process Intensification* 48 (3), 745 – 754.

List of publications

The results of this PhD thesis have been published in the following papers:

- Garcia-Gutierrez, L.M., Soria-Verdugo, A., García-Hernando, N. & Ruiz-Rivas, U. 2013 Simulation of object motion in a bubbling fluidized bed using a Monte Carlo method. *Chemical Engineering Science* 96, 26 - 32.

- Garcia-Gutierrez, L.M., Soria-Verdugo, A., Marugán-Cruz, C. & Ruiz-Rivas, U. 2014 Simulation and experimental study on the motion of non-reacting objects in the freeboard of a fluidized bed. *Powder Technology* 263 (0), 112 - 120.

- Garcia-Gutierrez, L.M., Soria-Verdugo, A. & Ruiz-Rivas, U. Optimization of the feeding ports location in a fluidized bed reactor based on Monte Carlo simulations of fuel particles. *Submitted for publication in Fuel.*

and presented in the following conference:

- Garcia-Gutierrez, L.M., Soria-Verdugo, A., Marugán-Cruz, C. & Ruiz-Rivas, U. 2013 Object motion in the freeboard of a bubbling fluidized bed. In *The 14th International Conference on Fluidization - From Fundamentals to Products,* pp. 591 - 598.

Other papers directly linked to this PhD thesis are:

- Soria-Verdugo, A., Garcia-Gutierrez, L.M., García-Hernando, N. & Ruiz-Rivas U. 2011 Buoyancy effects on objects moving in a bubbling fluidized bed. *Chemical Engineering Science* 66 (12), 2833 - 2841.

- Soria-Verdugo, A., Garcia-Gutierrez, L.M., Sánchez-Delgado, S. & Ruiz-Rivas, U. 2011 Circulation of an object immersed in a bubbling fluidized bed. *Chemical Engineering Science* 66 (1), 78 - 87.